Selective Emitter Materials and Designs for High-Temperature Thermophotovoltaic Applications

Ze Wang^{a,b}, David Kortge^{a,b}, Zihao He b , Jiawei Song c , Jie Zhu a,b , Changkyun Lee a,b , Haiyan Wang b,c,* and Peter Bermel a,b,*

ARTICLE INFO

Keywords: selective emitter thermophotovoltaics thermal stability multilayer filters photonics

ABSTRACT

In this manuscript, we review the role of selective emitters and filter materials in designs for thermophotovoltaics. After a brief review of the basics of thermophotovoltaics, we present a detailed discussion of options for highly-selective thermal emitters, highly-selective filters, and the interactions between them. We present a comprehensive analysis of 26 state-of-the-art selective emitters and discuss the particular advantages of each type of design strategy. We then discuss the fundamentals of materials stability, and how they can inform multilayer designs. We summarize the major challenges of current thermophotovoltaics with comparison to other competing energy conversion technologies. We then conclude with a summary and future perspectives on the prospects for highly-selective thermal emitters and filters.

1. Introduction

Thermophotovoltaic (TPV) technologies aim to convert heat into electricity via thermal radiation. While the technology was first discovered in 1956, and formal studies began in 1960, research still continues in search of designs offering a combination of high power, high efficiency, reasonable costs, and high reliability. A number of prior researchers have reviewed some of the key concepts and findings in thermophotovoltaics, up through the current era. To list a few past reviews [1–13]. In this review, we will aim to specifically focus on the interaction between materials and design for emitters and filters. As will be discussed in detail, there are both fundamental physical limits associated with the design of TPV systems, as well as major material challenges that require a fundamental understanding of the behavior of materials at high temperatures.

Early work on TPV showed that the performance was certainly bounded by the Carnot efficiency of heat engines, but TPV systems typically incur additional losses associated with the use of photovoltaics, which include sub-bandgap absorption, radiative recombination, and carrier thermalization. These factors point strongly to the need for operation at what are typically considered moderate to high temperatures; 700°C or above. Of course, many materials stable at room temperature experience phase changes and/or degradation when approaching such high temperatures, particularly in oxidizing atmospheres.

A range of material systems tolerant of moderate to high temperatures have been employed in TPV as thermal emitters. These include bulk refractory materials, rare earth materials, and photonic crystal designs. Each system has been found to have unique advantages and disadvantages. In general, bulk refractory materials offer low costs and some in-

Awang00@purdue.edu (H. Wang); pbermel@purdue.edu (P. Bermel)

band emission, rare earths offer a unique level of spectral selectivity, refractory metals offer low costs, and photonic crystals offer wavelength selectivity that can be tailored to the target application. Still, there are certain limitations associated with each system, which will be discussed further in Sections 3 and 6 of this review.

Selective filters provide another route to selectivity by reflecting back unwanted wavelengths via structures above or below the photovoltaic cell. The advantage is that they can operate at temperatures much closer to ambient, but must operate at some finite distance from the emitter, incurring losses associated with view factors less than unity. Selective filter-based designs developed by groups at Berkeley and Michigan have recently reported record radiation-to-electricity conversion efficiency of 29.1% [14] and 30% [15], respectively.

To better understand the considerations that go into the current and future record performance designs, the remainder of this paper is structured as follows. First, we will review the basic principles of thermophotovoltaics, then provide more details about highly-selective thermal emitters, highly-selective filters, and some trade-offs and interactions between these two components. Next, we will discuss the fundamentals of high-temperature thermal stability and provide design strategies for future multilayer selective thermal emitters and filters. We then discuss the challenges for current TPV systems and compare with other competing energy conversion technologies. We conclude with a summary and future perspectives of the field.

2. Principles of Thermophotovoltaics

A TPV system typically consists of four components: (1) heat source, (2) selective emitter, (3) spectral bandpass filter, and (4) photovoltaic (PV) cell [1], which usually can be planar or cylindrical, as shown in Fig. 1. Planar TPV is a com-

^aBirck Nanotechnology Center, Purdue University, West Lafayette, Indiana 47907, USA

^bSchool of Electrical and Computer Engineering, Purdue University, West Lafayette, Indiana 47907, USA

^cSchool of Materials Engineering, Purdue University, West Lafayette, Indiana 47907, USA

^{*}Corresponding author

mon structure which has been used in most of the research (Fig. 1(A)). It is easy to implement, but can potentially suffer a lower view factor. A cylindrical TPV can benefit from a near-unity view factor regardless of the distance between the emitter and PV cells, since the emitter is surrounded by PV cells from almost all directions (Fig. 1(B)). This ideally can minimize the view factor loss. However, a large PV surface area is needed, increasing the material costs as a result. Another type of cylindrical TPV, which is recently proposed conceptually for waste heat recycling [16], encompasses a pillar-shaped TPV cell with a round selective emitter (Fig. 1(C)). The emitter is heated by heat storage material, such as molten salt or PCM, which absorbs waste heat from high temperature industrial processes.

Thermal energy from the heat source is supplied to the emitter. Radiation from the emitter follows Planck's law of blackbody emission, given by:

$$\begin{split} P_{rad} &= A \int_{0}^{\infty} d\lambda \varepsilon_{e}(\lambda) I_{BB}(\lambda, T) \\ &= A \int_{0}^{\infty} d\lambda \frac{2\pi h c^{2}}{\lambda^{5}} \frac{\varepsilon_{e}(\lambda)}{e^{hc/\lambda kT} - 1}, \end{split} \tag{1}$$

where A is the surface area of the emitter, $\varepsilon_e(\lambda)$ is its emissivity at wavelength λ , and T is its temperature. $I_{BB}(\lambda,T)$ is the blackbody spectrum at T. The radiated photons are directed to the PV cell where the energy is converted to electricity. However, we note that the Planck's law does not capture near-field radiation effects [17]. The heat flow in a TPV system is shown in Fig. 2.

A number of sources of loss are present in the system. The overall efficiency, defined as the ratio of the output electrical power to the net input power, can be calculated as the product of component efficiencies, and is given by:

$$\eta_{\text{system}} = \eta_{\text{source}} \eta_{\text{ce}} \eta_{\text{ge}} \eta_{\text{ge}} \eta_{\text{oc}} \eta_{\text{ff}}$$
(2)

where $\eta_{\rm source}$ is the thermal efficiency of the heat source, $\eta_{\rm ce}$ is the cavity efficiency, $\eta_{\rm se}$ is the spectral efficiency, $\eta_{\rm qe}$ is the quantum efficiency, $\eta_{\rm oc}$ is the voltage factor, and $\eta_{\rm ff}$ is the fill factor. The key metrics and parameters are summarized in Table 1.

The energy input to the TPV system can be any heat source, such as chemical, solar, or nuclear. η_{source} is defined as the ratio of the net heat power received by the emitter to the total input power.

 $\eta_{\rm ce}$ is defined as the ratio of the net radiative heat absorbed by the cell to the net radiation from the emitter. It describes the effectiveness of emitter-cell integration, and is penalized by a non-unity view factor and/or photo-inactive areas on the cell.

Typically, thermal radiation photons are distributed across a broad range of energies. However, only photons at or above the bandgap energy, E_g , of the PV diode can be converted into electricity. The conversion of radiative heat absorbed by the cell into short-circuit current $J_{\rm sc}$ multiplied by the cell bandgap voltage $V_g = E_g/e_0$, defined as the bandgap

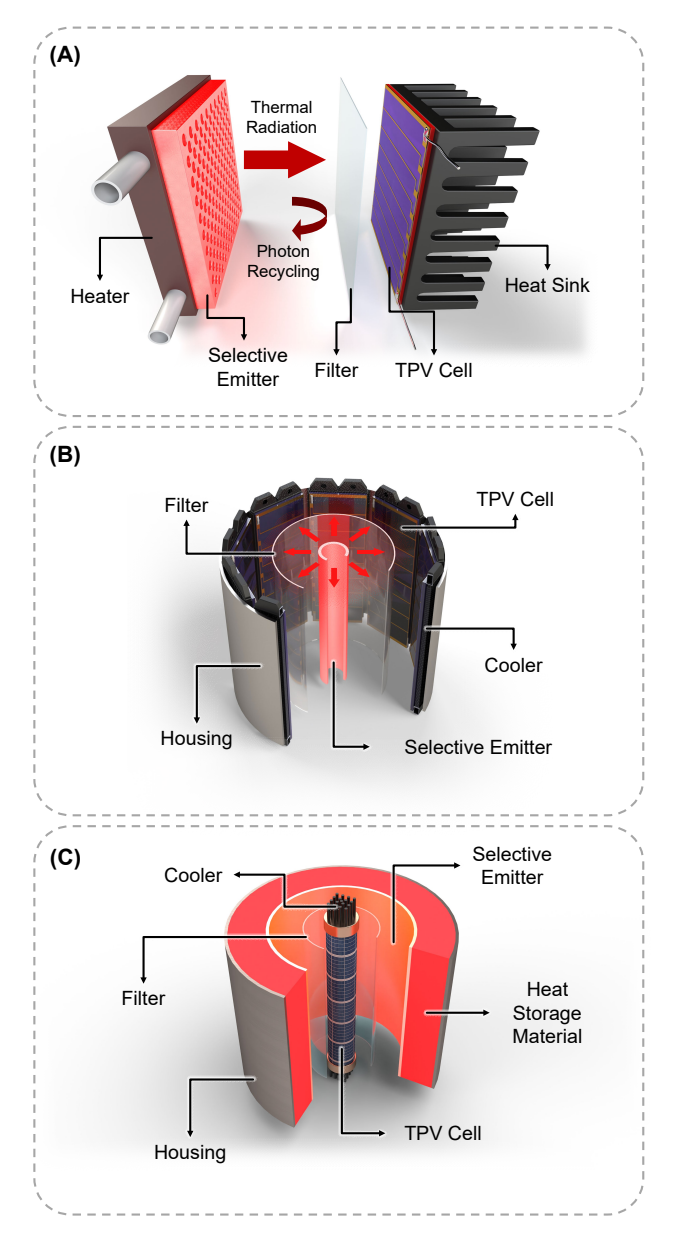


Figure 1: Three typical structures of TPV systems. (A) A flat TPV system. (B) A cutaway diagram of a cylindrical TPV system, where the emitter surrounds a heater. (C) Another type of cylindrical TPV system. The TPV cell is surrounded by an emitter. All structures include a heat source (e.g., a microcombustor), a selective emitter, a spectral filter, and a TPV cell. The heat source is thermally coupled with the selective emitter, converting heat to light with desirable wavelengths. The filter in front of the TPV cell rejects unwanted photons back to the emitter to further refine the spectrum of the incoming radiation. The TPV cell absorbs the filtered light and converts it into electricity. The heat sink or cooler keeps the TPV cell at low temperature to improve the performance.

energy divided by the elementary charge of an electron, is described by the product of spectral efficiency η_{se} and quan-

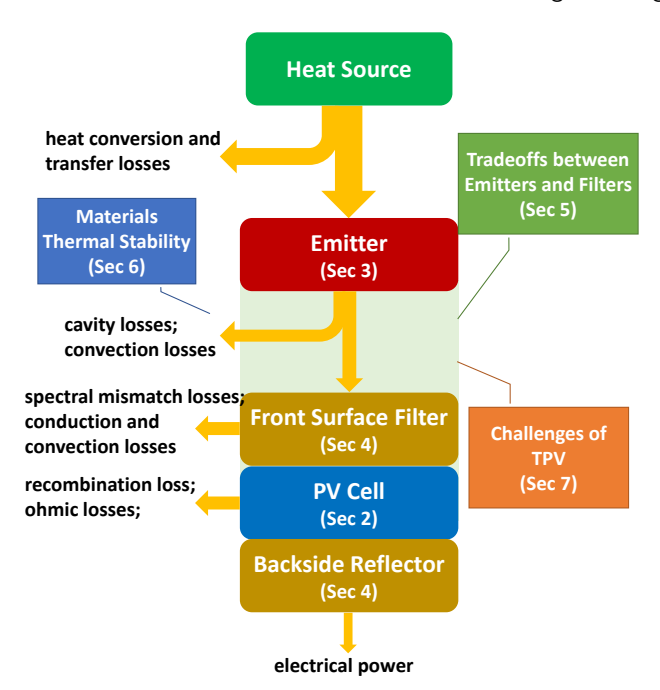


Figure 2: Heat transfer in a TPV system. The callout boxes summarize the main topics of this review.

Table 1
Key metrics and parameters in thermophotovoltaics

Parameter	Meaning
$\eta_{ m source}$	thermal efficiency of the heat source
$\eta_{ m ce}$	cavity efficiency
$\eta_{ m se}$	spectral efficiency
$\eta_{ m qe}$	quantum efficiency
$\eta_{ m oc}$	voltage factor
$\eta_{ m ff}$	fill factor
$\boldsymbol{arepsilon}_{\mathrm{e}}$	emitter emissivity
$\boldsymbol{arepsilon}_{\mathrm{c}}$	cell emissivity
$oldsymbol{arepsilon}_{ ext{eff}}$	emitter effective emissivity
$I_{ m BB}$	blackbody spectrum
$V_{ m OC}$	open-circuit voltage
$J_{ m SC}$	short-circuit current
$V_{ m g}$	cell bandgap voltage
$oldsymbol{J}_{ m ph}$	photocurrent density
$\dot{V_{ m m}}$	voltage at the peak power
$J_{ m m}$	current at the peak power
IQE	internal quantum efficiency
EQE	external quantum efficiency
$T_{ m e}$	emitter temperature
$T_{\rm c}$	cell temperature
$V_{ m th}$	thermal voltage

tum efficiency η_{qe} [11]

$$\eta_{\rm se}\eta_{\rm qe} = \frac{E_g \int_0^{\lambda_g} \varepsilon_{\rm eff}(\lambda) \cdot IQE \cdot b(\lambda, T) \, d\lambda}{\int_0^{\infty} \varepsilon_{\rm eff}(\lambda) \cdot E \cdot b(\lambda, T) \, d\lambda},\tag{3}$$

where E is the photon energy, $b(\lambda,T)$ is the spectral photon flux of a blackbody, and IQE is internal quantum efficiency. $\varepsilon_{\text{eff}} = \frac{\varepsilon_e \varepsilon_c}{\varepsilon_e + \varepsilon_c - \varepsilon_e \varepsilon_c}$ is the effective emissivity of the

cavity formed by the emitter and the cell, accounting for multiple reflections between the emitter and the cell, where ε_{o} and ε_c are emitter and cell emissivity, respectively. There are two main loss mechanisms associated with spectral mismatch between the emitter and the cell: free carrier heating and phonon absorption due to absorption of below-bandgap energy photons that are not converted to electrical energy, and hot carrier heating due to absorption of photons with energies well above the bandgap energy. To minimize wasted energy, spectrally selective emitters with enhanced emission above the PV bandgap can be introduced. A bandpass filter between the emitter and the cell can further reduce the losses by rejecting sub-bandgap photons and recycling them back into the emitter. Additionally, a backside reflector reflecting the out-of-band (OOB) photons back to the emitter can be used to further enhance efficiency.

An ideal photovoltaic cell can be modeled as a constant current source in parallel with a diode. When the cell is in the dark, there is no contribution to the current generation and photocurrent density, $J_{\rm ph}$, will be zero; this is a general characteristic of PV cells [1]. When the cell is under illumination, each absorbed photon above the PV cell bandgap energy generates photocurrent which shifts the current-voltage curve to the fourth quadrant (Fig. 3). The I-V relation of the illuminated diode has the form [18],

$$J(V) = \int_0^{\lambda} \lambda \left[\frac{2e_0 c}{\lambda^4} \frac{\epsilon_e(\lambda) EQE(\lambda)}{\exp(hc/\lambda kT_e) - 1} \right]$$

$$- \left[\frac{q(n^2 + 1)E_g^2 kT_c}{4\pi^2 \hbar^3 c^2} e^{-E_g/mkT_c} + J_{\rm nr} \right]$$

$$\times (e^{qV/mkT_c} - 1)$$

$$(4)$$

where k is Boltzmann's constant, $h=2\pi\hbar$ is Planck's constant, c is the speed of light, λ is the wavelength, $EQE(\lambda)$ is the external quantum efficiency of the TPV device, $\varepsilon(\lambda)$ is the emissivity of the selective emitter, T_e is the temperature of the emitter, E_g is the bandgap of the TPV device, m is the device ideality factor, T_d is the device temperature, n is the refractive index of the TPV semiconductor region, and J_{nr} is the dark current density induced by nonradiative recombination.

The open-circuit voltage $V_{\rm oc}$ is the voltage when the current is equal to zero in the diode (i.e., when the circuit is open). The maximum voltage obtained from the PV cell is the bandgap voltage V_g . The voltage factor is defined as $\eta_{\rm oc} = V_{\rm oc}/V_g$, i.e., the ratio of open-circuit voltage to the bandgap voltage. It serves as a measure of the efficiency of utilization of the bandgap energy.

The open-circuit voltage increases with the photocurrent density $J_{\rm ph}$, or the reduction of dark saturation current density, J_s , which, in turn, increases the voltage factor. As shown in Figure 4, PV cells made of gallium antimonide (GaSb), germanium (Ge), and indium gallium arsenide (InGaAs) generally have higher performance because of their relatively high voltage factors and modest bandgap energies, which benefit most of the TPV cells [1]. The trends of voltage factor reduction at lower bandgap for both one-sun and con-

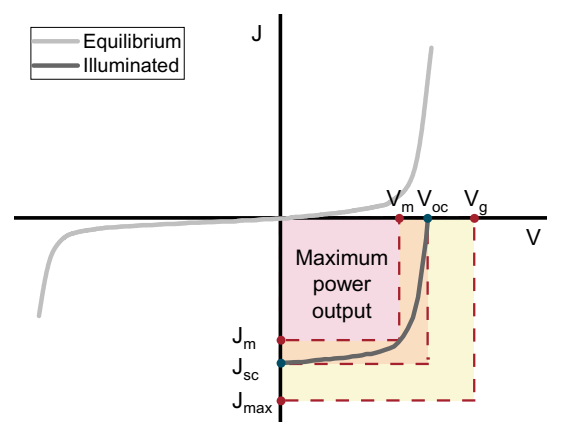


Figure 3: Characteristic curve of current versus voltage in a TPV cell. Adapted from [1]. $J_{\rm m}$ and $V_{\rm m}$ are the output current and voltage at the maximum power point; $J_{\rm sc}$ and $V_{\rm oc}$ are the short-circuit current and open-circuit voltage; $V_{\rm g}$ and $J_{\rm max}$ are the bandgap of solar cell and the corresponding maximum current density.

centrated conditions are fitted as the blue and red curves, respectively, with an empirical model given by [1]

$$\eta_{OC,empirical} = \frac{V_{OC}}{V_g} = \frac{hv_g - hv_0}{hv_g},\tag{5}$$

where hv_0 is taken as 0.35 eV at one sun, empirically, and 0.25 eV at concentration factors higher than 100. Another important information illustrated in the figure is that higher concentration level can typically improve the voltage factor (this can be seen by comparing GaSb and Si), which is beneficial for TPV applications.

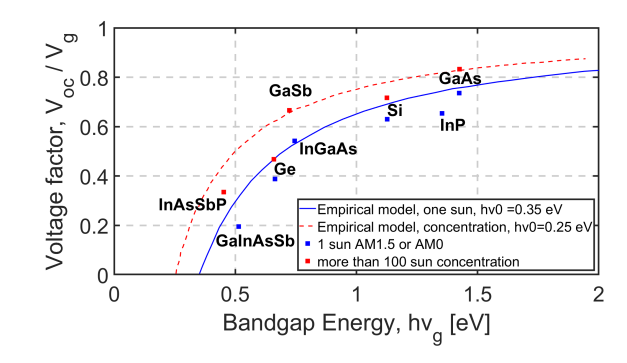


Figure 4: Voltage factor vs bandgap for different concentration levels. The blue and red curves fitting the trend of voltage factor at different concentration levels are plotted, respectively. Adapted from [1].

Since the current-voltage curve of the PV cell under illumination follows an exponential function (ignoring series resistance for now), the peak electrical power density $J_m V_m$ is thus less than $J_{sc}V_{oc}$. This is described by the fill factor

$$\eta_{\rm ff} = \frac{J_m V_m}{J_{\rm SC} V_{\rm OC}}.\tag{6}$$

Fill factor deteriorates with low open-circuit voltage [19, 20] and high cell temperature [21], as well as non-ideal series and shunt resistances [22–25]. Figure 5 shows the practical fill factor values of different PV cells as a function of open circuit voltage normalized by the thermal voltage, where $V_{\rm th} = kT_c/e_0$ [13]. For the best performance, PV cells should be designed with low series and high shunt resistance values.

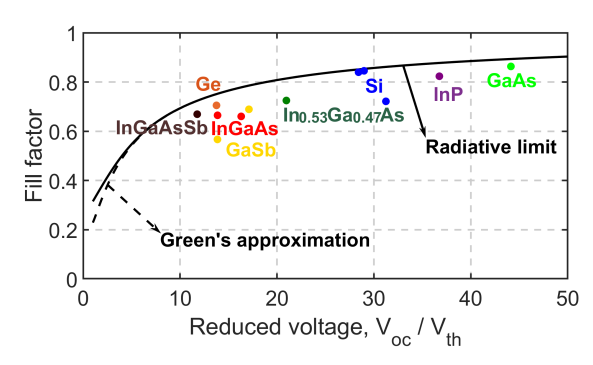


Figure 5: Fill factor vs open-circuit voltage normalized by thermal voltage for high-performance TPV and PV cells (one sun), compared to the theoretical Shockley-Queisser limit (solid line) [19] and empirical model developed by Green (dashed line) [20]. Adapted from [1].

Among the popular choices of PV cells, silicon and germanium cells were first demonstrated in the application of TPV [26]. Ge cells have an indirect bandgap of $E_g = 0.66$ eV at room temperature, and its cost is much lower than III-V semiconductors. Silicon has a relatively high bandgap of $E_g = 1.12$ eV, and thus is only suitable for high temperature PV system [27]. The most popular choices in the TPV literature are III-V semiconductors, typically GaSb (0.7 eV), In-GaAs (0.6–0.7 eV), and InGaAsSb (0.5–0.6 eV). The fabrication technique for GaSb cells is mature, but GaSb cells exhibit high dark current densities attributed to recombination centers introduced during doping. InGaAs and InGaAsSb PV cells are fabricated by epitaxial growth and are not yet commercialized, but their low bandgap matches well with some rare-earth emitters [9].

At the system level, TPV usually works in more severe environments than other PV-based technologies such as flatpanel PV and concentrating photovoltaic (CPV) systems [28] since (1) TPV systems typically operate in vacuum with limited convection; (2) emitters are often heated up to 1500 °C; and (3) smaller bandgap results in greater sensitivity of the open voltage to elevated temperature. Thus, cooling constraint is an important consideration. Active cooling is often used for TPV cell thermal management, which can be effective but also complex, cumbersome, and requires extra power consumption. Among water cooling and air cooling, water has higher heat transfer rate, but it is more difficult to design as a reliable system, and water may damage electronics [21]. Recently, radiative cooling has been reported as a lightweight, compact, and passive cooling method which has been demonstrated in several CPV systems with considerable temperature drops [29, 30]. These results suggest that

radiative cooling can be a good candidate for high-temperature TPV and solar TPV (STPV) systems due to their shared similarities with CPV.

3. Highly Selective Thermal Emitters

In principle, a selective emitter for TPV systems should have a unity in-band emissivity and zero elsewhere, since photons below the bandgap of PV cell cannot be converted into electricity. Out-of-band photons are not only useless but can also heat up the PV cell, resulting in lower efficiency and lifetime, which should be avoided in all cases. Optimizing the in-band emissivity, however, is a more interesting topic. Due to the thermalization loss in PN junctions, the extra above-bandgap energy carried by a photon cannot be extracted as electricity either, making these photons unwanted in certain cases as well. Therefore, photons having energy slightly greater than the bandgap are ideal for PV cells, which leads to the concept of narrow-band selective emitters to maximize the radiation-to-electricity efficiency. However, a narrower emission range can reduce the radiation power density, leading to lower power output. There is always a trade-off between efficiency and power density for TPV systems. A sketch showing the comparison of ideal broad-band and narrow-band emitters is illustrated in Fig. 6.

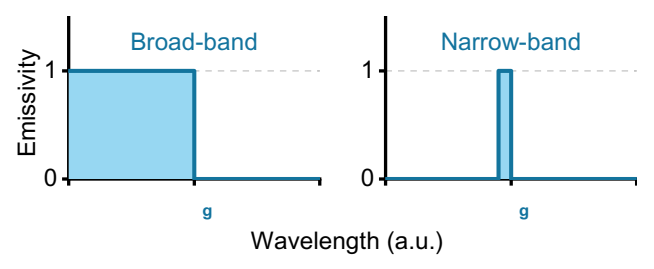


Figure 6: A comparison between two types of emitters. λ_g is the bandgap of PV cell. The broad-band emitter aims to maximize the radiation power density, while a narrow-band selective emitter aims to maximize the radiation-to-electricity efficiency.

Selective emitters have been investigated extensively in the past few decades [31–62]. Broadly speaking, there are two ways of designing an emitter. In pursuit of an adequate optical performance, one can either take advantage of the intrinsic optical properties by finding the right materials, which naturally have a certain spectrum selectivity (e.g., rare-earth metals), or use a broad-band emitter and reshape its emissivity by changing the surface structure (e.g., anti-reflection coating, photonic crystal). The two approaches can also be combined if needed.

Although a variety of structures for selective emitters have been reported, they can generally be classified into three categories, as illustrated in Fig. 7: (a) bulk emitters, (b) rareearth composite or doped emitters, and (c) photonic crystal (PhC) emitters. We will walk through the details of each type of the emitters in this section. We note that certain emitter proprieties (cut-off wavelength, spectral efficiency, etc.) we report in the following may differ from the original publications, since we re-evaluated them using a more consis-

tent calculation method which will be introduced thoroughly later. Fig. 8 shows some of the most representative selective emitters and associated TPV systems that have been experimentally fabricated in recent years.

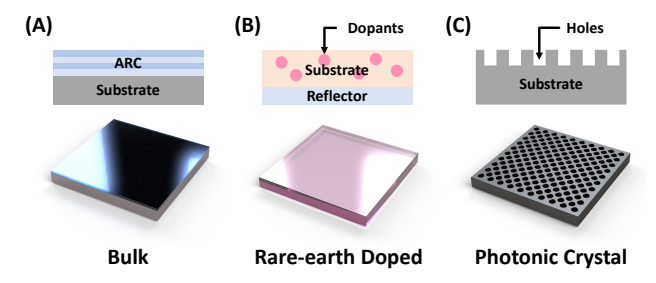


Figure 7: A scheme of three types of selective emitters classified by the structure. (A) Emitter made from bulk materials, such as Si, SiC, W, etc., usually fabricated with anti-reflective coating to enhance the in-band emission. (B) Rare-earth metal doped emitters. YAG is a common substrate material, which displays good thermal stability and low IR emissivity. Rare-earth emitters can also be composite bulk material or fibrous mantle, which are not plotted here. (C) 2D Photonic crystal emitters. The emitting surface is etched with periodic micrometer-sized holes to improve in-band radiation. Holes are enlarged in the figure for readability.

Bulk refractory emitters [32, 46, 54, 55] are widely available and easy to fabricate. They naturally have broad-band, intrinsic emissivity. Materials such as tungsten (W), tantalum (Ta), silicon (Si), silicon carbide (SiC), etc. have been commonly used in literature. However, they are often not highly selective without additional photonic structures. Refractory semiconductors have some bandgap-based selectivity, but are subject to free carrier absorption at longer wavelengths, particularly for thicker substrates. Typically, introducing an anti-reflection coating (ARC) or other photonic structures can enhance in-band thermal radiation. For instance, Shimizu et al. [54] demonstrated a monolithic tungsten selective absorber/emitter (Fig. 8(K)) for STPV system with yttria-stabilized zirconia (YSZ) coated on both sides as ARCs. The coating structure on the top surface was designed to enhance solar absorption, while the bottom one was refined as a thermal emitter for a GaSb solar cell. A groundbreaking system efficiency (solar-to-electricity) around 8% was experimentally achieved in 2015. Later in the same year, another tungsten absorber/emitter for STPV was experimentally demonstrated with a system efficiency of 6.2% [55]. While sharing a similar structure as the previous work on the emitter side (W emitter with Si₃N₄ ARC), the absorber's surface was unique. A small area in the middle of the absorber was laser-textured to improve solar absorption, while the rest surrounding area remained as polished tungsten surface with low emissivity. An IR mirror with a hole cut in the middle was placed toward the top surface to minimize the thermal radiation loss from the absorber without blocking solar input. However, many of these systems are susceptible to rapid degradation at high temperatures for atmospheric levels of oxygen, so they must operate in high or

ultra-high vacuum conditions.

Rare-earth elements exhibit atom-like transitions with narrow peaks in the IR region – most famously, erbium around 1.5 microns, which sometimes match well with modest-bandgap PV cells, such as GaSb and InGaAsSb. This unique property gives intrinsic spectral selectivity and has thus attracted much attention for TPV applications. Rare-earth emitters are relatively easy to fabricate at large scale by doping ceramics, and can usually deliver excellent thermal stability due to the monolithic structure. For best performance, they often require embedded in expensive substrates, such as yttrium aluminum garnet (YAG). Those embedded in oxides may have reasonable tolerance for oxidizing environments. Although the intrinsic peak wavelength is not tunable, researchers are able to add multiple dopants or synthesize composites to obtain more peaks [33]. Among different elements, Er, Yb, and Ho were studied quite frequently [31, 33-36, 38] due to their desirable emissivity. A common structure of rareearth emitter in early cylindrical TPV prototypes possesses a special "Welsbach" mantle structure (Fig. 8(A)), inspired by an incandescent gas mantle [36, 38, 47]. The fabrication follows the Bauer/Nelson process, which produces fibrous ceramic mesh. The emitters are resilient to thermal shock, enabling good stability in high temperatures. However, they are extremely fragile and cannot survive a simple bend test [40]. Compared with the mantle structure, rareearth-doped ceramics show promising mechanical properties. Lowe et al. reported Er and Ho doped YAG emitters in early works [31, 33] showing a good spectral selectivity. The peak emissivity reached between 0.6 to 0.8. Later, plasmaspray coated Er and Yb emitters were studied by Tobler et al. [41, 42]. Er₂O₃ and Yb₂O₃ were deposited on MoSi₂ substrates, which share a similar thermal expansion coefficient and high melting temperature. For that reason, the emitters were tested at temperatures up to 1923 K and showed no delamination. More importantly, they are fully able to operate in oxidizing atmospheres. Composite rare-earth emitters have also been investigated. Adair et al. fabricated several emitters with paper-making techniques in their work [34]. The advantage of this method is the ability to produce geometries in any shape. Composite samples consisting of quartz, cellulose, carbon, and Nextel fibers were formed together with Er₂O₃, Ho₂O₃, and Yb₂O₃, respectively, and tested at 1640 K. Another Al₂O₃ / Er₃Al₅O₁₂ composite emitter presented by Yugami et al.[35] was experimentally tested in a GaSb STPV system at 550 K. Although the spectral efficiency of the emitter reached an acceptable value of \sim 34%, the system efficiency was only \sim 0.02%, which was likely caused by the low operating temperature and view factor loss. In fact, most of the aforementioned rare-earth-based emitters are not able to provide a remarkable spectral efficiency. The typical values fall between 20% to 50%. The reason partially pertains to the narrow emission peak and considerable out-of-band background radiation from the structural material.

Photonic crystals, as one of the most popular technologies in optics, have shown a promising future in TPV appli-

cations. The emergence of nanophotonics has made it possible to tailor emissivity spectra more precisely than ever before [63]. PhC emitters use periodic surface microstructures to enhance thermal radiation within the target wavelength range. The structure can be 1D, 2D, or 3D. While 1D and 2D PhC emitters are widely reported in many works, 3D PhC emitters are rare, presumably due to the complicated fabrication process and limited performance improvement.

A 1D PhC contains periodic planar layers made from at least two different materials, which resembles an ARC or multilayer stack (with no periodicity). In 2013, Chan et al. [48] fabricated a Si/SiO₂ 1D PhC emitter and combined it with a micro-combustor InGaAsSb TPV (Figs. 8(I) and (M)). The operating temperature was maintained at 1073 K with a maximum system efficiency of 2.5%. A later work performed by Lenert et al. [51] applied the same Si/SiO₂ 1D PhC emitter (Figs. 8(I)) into a STPV system, reaching a system efficiency of 3.2% at 1285 K. In 2016, Bierman et al. [64] integrated the same emitter into a refined STPV system with a rugate filter, reached a system efficiency of 6.8% at 1273K. Multilayer stacks are similar to 1D PhC emitters, therefore are also discussed here. Kohiyama et al. reported a Mo/HfO₂ multilayer stack emitter in 2016 [56], which achieved a 5.1% system efficiency at 1640 K in a GaSb STPV system. In 2019, a metamaterial emitter, which has a smaller feature size than 1D PhC, was reported by Chirumamilla et al. [60]. The emitter consists of periodic 1D HfO_2/W layers at ~20 nm scale (Figs. 8(J)), giving a very high spectral efficiency of 80%. The emitter was examined at 1673K for 6 hours, showing slight degradation only. A most recent work in 2020 from Bhatt et al. has reached a recordhigh system efficiency of 8.4% in a GaSb STPV system [62]. The emitter is made of a 4-layer W-Si₃N₄ stack with lasertextured top surface to increase solar absorptance. Both the emitter's spectral efficiency and in-band power density are high, holding a value of 74% and 13.9 W/cm², respectively.

2D PhCs are usually fabricated by etching periodic holes on the emitting surface. By changing the diameter and spacing of the holes, the emissivity can be adjusted to a desirable profile with greater versatility than many other methods. One advantage of 2D over 1D PhCs is the potentially better thermal shock resistance thanks to the monolithic structure [61]. If the periodic patterns are properly designed, a fairly good emissivity can be obtained without any ARC, eliminating the risks of delaminations caused by mismatch of thermal expansion coefficients. Many recent papers have explored the possibilities of 2D PhC emitters [43–45, 49, 52, 57, 59]. Tungsten and tantalum are the most common substrate materials, since they exhibit excellent thermal stability and low out-of-band emissivity. According to the published data, the spectral efficiency of 2D PhC emitters can vary between $\sim 30\%$ to $\sim 65\%$, which generally perform better than rare-earth emitters. Araghchini et al. [43] and Yeng et al. [45] reported tungsten 2D PhC emitters in two separate studies (Fig. 8(B)). The operating temperature was designed at 1230 K for both works, with spectral efficiency of 31% and 45%, respectively. The emitter from Yeng's work was also

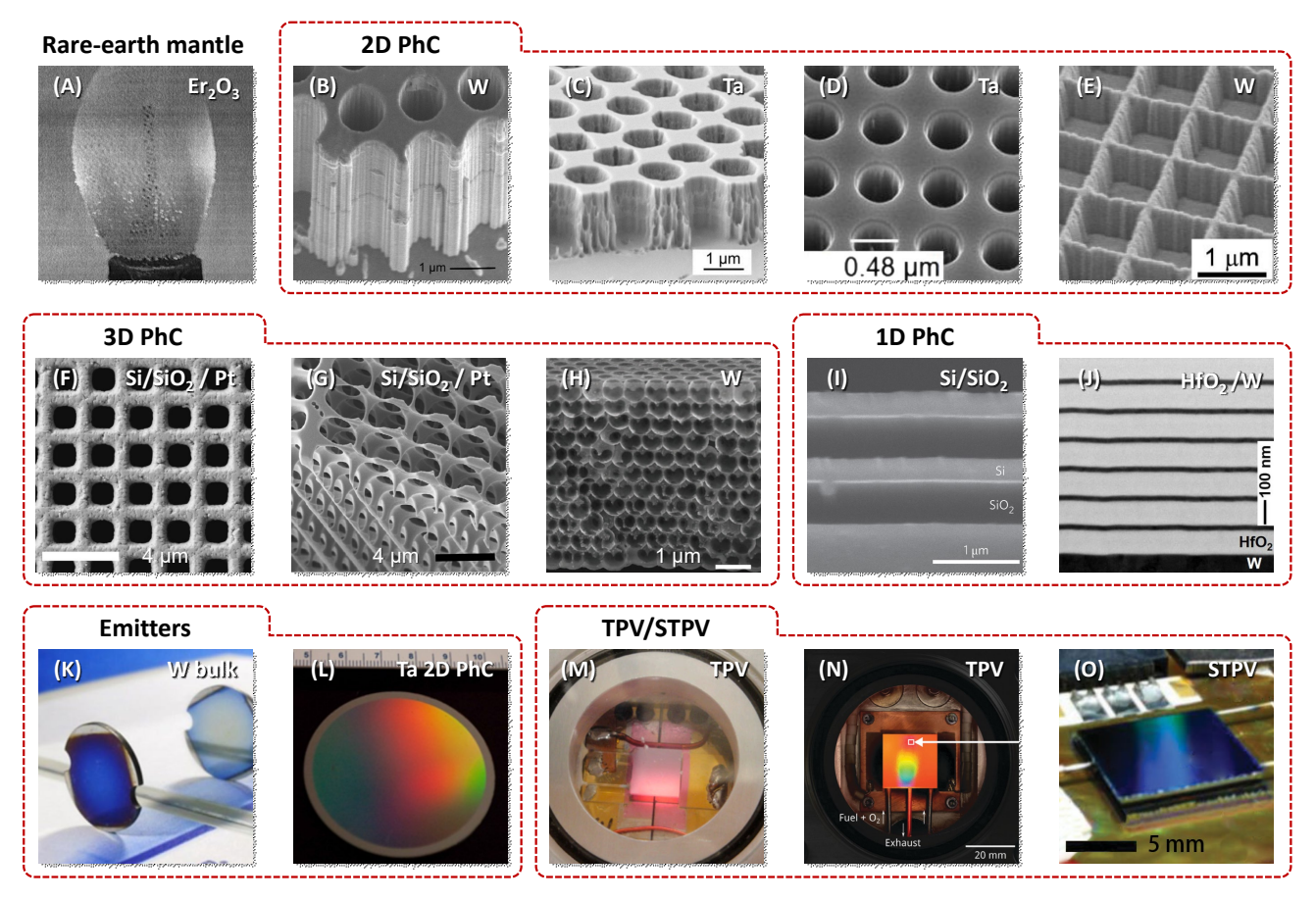


Figure 8: Photos of fabricated emitters and TPV/STPV systems grouped by types. The emitter material is noted in the top-right corner in each panel. (A) A photo of a typical rare-earth mantle emitter [38]. (B)-(E) Scanning electron microscope (SEM) images of 2D PhC emitters. Each has a unique pattern, size, and aspect ratio [39, 45, 49, 52]. Flat surface with periodic holes is a common pattern for 2D PhCs. (F)-(H) SEM images of 3D PhC emitters [50, 53]. The first two images show the same emitter from different angles. (I)-(J) SEM images of 1D PhC/metamaterial emitters [48, 51, 60]. (K)-(L) Photos of different types of emitters [44, 54]. The front surface in (K) is the absorber and the back surface (shown in the mirror) is the emitter. The diffraction pattern in (L) is caused by surface microstructure. (M)-(O) Photos showing emitters sitting in TPV/STPV systems [48, 52, 57], typically in vacuum chambers. The reddish glowing in (M) [48] is caused by high-temperature thermal radiation. Rainbow-like color in (N) [57] is diffraction pattern. The blue surface in (O) [52] is a solar absorber. The emitter side is facing down toward an InGaAsSb PV cell. All figures are reprinted with permissions from [38] © 2002 Elsevier Science B.V.; [49] © 2013 Optical Society of America; [45] © 2012 National Academy of Sciences; [52] © 2014 WILEY-VCH Verlag GmbH & Co. KGaA, Weinheim; [39] © American Institute of Physics; [53] © 2014 Elsevier B.V.; [50] © 2013 Macmillan Publishers Limited; [51] © 2014 Macmillan Publishers Limited.; [60] © The Author(s) 2019; [54] © 2015 Society of Photo-Optical Instrumentation Engineers (SPIE); [65] © 2013 American Vacuum Society; [48] © 2013 National Academy of Sciences; [57] © The Royal Society of Chemistry 2017; [52] © 2014 WILEY-VCH Verlag GmbH & Co. KGaA, Weinheim.

tested over 10 hours in vacuum at 1200 K, showing no measurable degradation. Rinnerbauer et al. had been working on tantalum 2D PhC emitters in several publications (Figs. 8(C) and (D)) [44, 49, 52]. The working temperatures varied from ~1200 to 1300 K, with a maximum spectral efficiency of 52%. One of the emitters was tested for 144 hours in vacuum at 1173 K [49]. While no sign of degradation was observed for in-band radiation, the out-of-band radiation increased by a factor of ~4 after 24 hours and became stabilized. Another emitter was tested in an InGaAsSb STPV system (Fig. 8(O)) providing an system efficiency of 3.74% [52]. In a later work, Chan et al. [57] demonstrated a similar Tantalum 2D PhC emitter in an InGaAsSb TPV system (Fig.

8(N)), reaching an unprecedented system efficiency of 4.4% (note that this efficiency is for TPV instead of STPV, unlike the work from Bhatt et al. [62]). The thermal stability was also tested for 100 hours in vacuum under 1173 K showing no degradation. A recent work from Suemitsu et al. [66] reported a Si-rod 2D PhC emitter sitting on top of a MgO substrate. The emitter was tested in an InGaAs TPV showing a system efficiency of 11.2% under 1338K. However, the heat source is an electrically heated Pt/Ti wire without any exhaust or optical losses like usual TPV/STPV systems in other works. The system efficiency may drop if using a combustor.

3D PhCs provide the possibility of fully tuning the spec-

Table 2 Evaluation parameters for emitter performance. Specially, the value of M_{in} , M_{out} , ε_{in} , and ε_{out} are calculated at the corresponding operating temperature T. η_{se} is defined by assuming paring the emitter to an ideal PV cell with bandgap of λ_c , EQE=1, and no thermalization and view factor losses, which is an ideal case of η_{se} discussed in Section 2.

Notation	Value	Unit	Description
ϵ_e	reported	[1]	emitter emissivity
I_e	reported	[W/m²/ nm/str]	spectral radiance
T	reported	[K]	operating temperature
M_{in}	$\pi \int_0^{\lambda_c} I_e \mathrm{d}\lambda$	$[W/cm^2]$	in-band radiance
M_{out}	$\pi \int_{\lambda_c}^{\infty} I_e \mathrm{d}\lambda$	$[W/cm^2]$	out-of-band radiance
$\varepsilon_{\it in}$	$\int_0^{\lambda_c} I_e/I_{bb} \mathrm{d}\lambda$	[1]	in-band emissivity
ε_{out}	$\int_{\lambda_c}^{\infty} I_e/I_{bb} \mathrm{d}\lambda$	[1]	out-of-band emissivity
η_{se}	$M_{in}/\left(M_{in}+M_{out}\right)$	[1]	spectral efficiency

trum of an emitter, but are less reported in literature. In 2015, Garin et al. [53] fabricated a Si/SiO₂/Pt 3D PhC emitter (Figs. 8(F) and (G)) with a spectral efficiency of 49% at 1100 K. No noticeable changes were observed after an 8-hour durability test in N₂ at 1100 K. Another study from Arpin et al. [50] reported a HfO₂-coated W 3D PhC emitter (Fig. 8(H)). The coating can effectively protect the emitter from thermal degradation. A slight increase of out-of-band radiation was observed after annealing at 1627 K for 1h. The spectral efficiency is 67% with a high in-band radiance at 20.3 W/cm² Nonetheless, both emitters were not experimentally tested in TPV/STPV systems.

A list summarizing the performance of the aforementioned emitters can be found in Table 3. Since each individual work measured and calculated the emitter properties in different methods, making a direct side-by-side comparison would be difficult. In addition, parameters used in the calculations from reported works, such as cut-off wavelength, spectral efficiency, etc., are often attributed to the PV cells or target values, which do not reflect the real properties of the emitters. Thus, in order to make a somewhat fairer comparison, we extracted the emissivity (or radiance) data from each publication and evaluated their performances in a consistent manner. Specifically, we treat the emitters as broadband. The in-band radiation range thus extends from 0 µm to the wavelength at which the emissivity drops below 0.5 (but less than 2.5 µm, which can still match some modestbandgap materials such as InGaAs). Therefore, the data calculated and shown in Table 3 may differ from the ones published in the original works or other review articles. Metrics for emitters include material, angle θ at which the emissivity or radiance is measured, cutoff wavelength λ_c , peak

power density wavelength λ_{peak} , in-band emissivity ε_{in} , outof-band emissivity ε_{out} , spectral efficiency η_{se} , in-band radiance M_{in} , operating temperature T, and thermal stability test results. Moreover, for works with emitter-PV pair demonstrations, the system type, PV material, PV bandgap λ_g , and reported overall system efficiency η_{sys} (fuel-to-electricity for TPV, solar-to-electricity for STPV) are also included in Table 3. Emissivity is often angular-dependent, which typically peaks at normal incident angle and gradually reduces to near-zero at $\sim 90^{\circ}$. This property can be seen in many works [52, 53, 58, 59] where the angular-dependent emissivities are reported. Among the emitters in the list, most of the emssivities are measured at normal incident angle (peak emissivity). The real optical performance is therefore likely to be worse than the calculated values. We note that the values listed in the table are only for reference and not exact, since the emissivity (or radiance) data can be obtained at different angles and temperatures for different structures, which may introduce errors in the comparison.

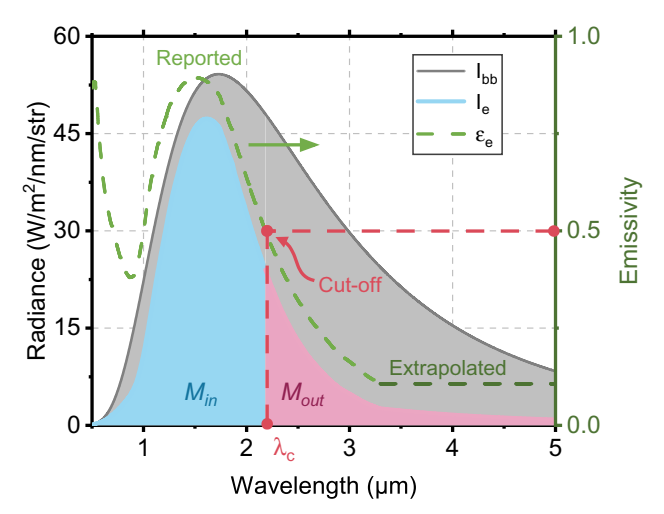
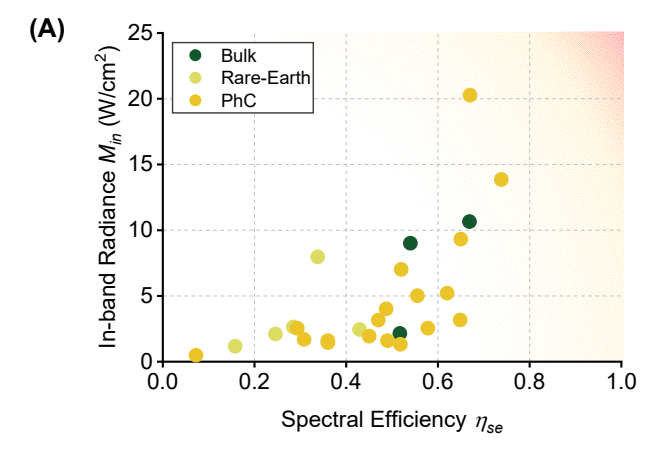


Figure 9: A sketch showing how the key parameters are processed in the performance evaluation. The cut-off wavelength at where the emissivity (green curve) drops below 0.5 is noted as λ_c ; spectral radiances of the emitter (I_e , blue/pink curve) and the black body (I_{bb} , gray curve) are plotted at T=1676~K; M_{in} and M_{out} are the integrated in-band and out-of-band radiance, respectively. The emissivity beyond reported wavelength is interpolated as the boundary value (dark green). Data is extracted from [62].

The calculation method is illustrated in Fig. 9. First, we extract the emitter's emissivity (ε_e) or radiance data (I_e) from the previously introduced publications. The emissivity is then extrapolated from $0\,\mu\mathrm{m}$ to $100\,\mu\mathrm{m}$ using the boundary values. The error caused by extrapolation is generally well-bounded, since most of the radiation power falls into the reported wavelength ranges in the majority of cases. The cut-off wavelength (λ_c) is then determined by finding the spot at which emissivity drops below 0.5. The in-band and out-of-band radiance $(M_{in}$ and $M_{out})$ as well as emissivity $(\varepsilon_{in}$ and $\varepsilon_{out})$ are calculated at the reported operating temperature T. The mathematical definition of the above parameters are

listed in Table 2. Specifically, the calculation for spectral efficiency η_{se} effectively assumes that: (1) the pairing PV cell has a bandgap of λ_c with ideal EQE (i.e., EQE=0 for out-of-band photons, EQE=1 for in-band photons), (2) no thermalization loss in PV cell, and (3) view factor and parasitic heat losses are zero. The assumption simplifies η_{se} shown in Eq. 3 and only considers the emitter itself in ideal working conditions.



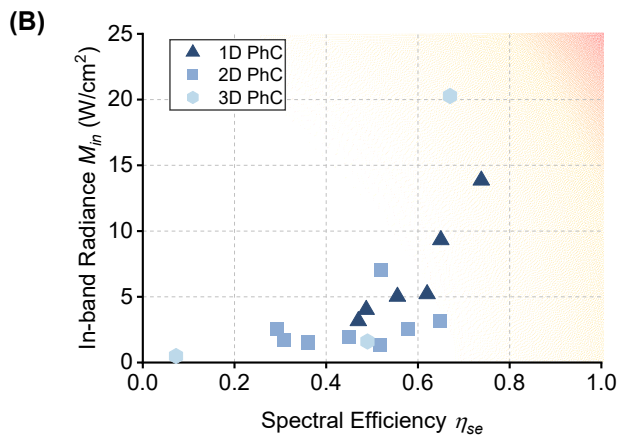


Figure 10: A comparison of spectral efficiency η_{se} and in-band radiance M_{in} for emitters shown in Table 3. The top-right corner indicates better optical performance with both high η_{se} and M_{in} . (A) All discussed emitters grouped by type. Note that PhC emitters shown here also include multilayer stack and metamaterial emitters. (B) A closer look at PhC emitters with different structures (including multilayer stack and metamaterial emitters).

A lot of information can be obtained from the side-byside comparison in Table 3. To achieve high spectral efficiency η_{se} , the in-band emissivity ε_{in} , operating temperature T, and cut-off wavelength λ_c should be as high as possible (but without exceeding far beyond the bandgap of the TPV cell, e.g., becoming a black body emitter), while keeping the out-of-band emissivity ε_{out} low. Some interesting comparative results can be found. For example, emitter O [51] holds the highest in-band emissivity (0.88), yet the spectral efficiency is relatively low (0.49). This is caused by a high out-of-band emissivity (0.39) which cancels out the in-band emission. A similar example is emitter M [48]. On the contrary, emitter Z [62] has a lower ε_{in} of 0.75, while the overall spectral efficiency is high, due to the lower ε_{out} . Nonetheless, if we compare emitter Z [62] with U [57], the latter has a better performance for both ε_{in} and ε_{out} , yet the η_{se} is lower than emitter U [56]. This is caused by a lower operating temperature (can affect the shape of spectrum, red-shifting the energy distribution) and cut-off wavelength. To design a high-performance selective emitter, one should not only focus on in-band emissivity ε_{in} or spectral efficiency η_{se} , but also the absolute in-band radiance M_{in} to increase the total generated electricity. An interesting comparison that shows the importance of temperature can be seen in emitters P [52] and R [54]. They both have the same ε_{in} of 0.83 and similar λ_c , while the radiance M_{in} from emitter R [54] is almost 4 times higher because of the increased operating temperature. Another comparison is between emitter T [56] and emitter Z [62], where ε_{in} and temperature are similar in both cases, but M_{in} for emitter Z [62] is more than double that for T, since λ_c is longer.

Fig. 10 shows the two most important parameters, namely, spectral efficiency η_{se} and in-band radiance M_{in} , of the selective emitters discussed in Table 3. As can be seen in Fig. 10(A), emitters sitting closer to the top-right corner have better optical performances with both high efficiency η_{so} and power density M_{in} , which are essential for high performance TPV systems. Most of the reported emitters cannot achieve an in-band radiance above 5 W/cm², although some of them may have remarkable spectral efficiencies. Obtaining a high in-band power density seems difficult, since it usually requires both a high operating temperature and an excellent spectral efficiency. In terms of emitters' structure, PhC (including multilayer stack and metamaterial) emitters appear to be the most popular choices according to published works in the past two decades. PhC and bulk emitters generally outperform rare-earth emitters, while the latter may have a better thermal stability. To take a closer look at the PhC emitters, we plot Fig. 10(B) to show the performance of 1D, 2D and 3D PhC emitters in the same manner as Fig. 10(A). As can be seen, having a higher dimension in the structure design does not necessarily lead to a better optical performance. Instead, 1D PhC and multilayer stack emitters seem to exhibit more appealing results. However, they may suffer a worse thermal degradation due to the multilayer structure. On the other hand, most of the 2D PhC emitters have been thermally tested with positive results. The limitations and trade-offs for high-performance selective emitters should be carefully evaluated based on the design goals.

At the system level, fuel-burning TPV usually displays a lower overall efficiency (fuel-to-electricity) than STPV, mainly owing to the huge energy loss from exhaust heat in TPV's combustor. Whereas in an STPV system, the efficiency is evaluated as the input solar radiation power to the electricity output, which avoids the parasitic heat loss in fuel combustion. For that reason, we do not recommend using the system efficiency as an emitter's performance indicator.

In addition to the practical demonstrations discussed above,

recent simulation works have shown greater freedom in emitter designs. In particular, rare-earth-doped YAG [67], 1D PhCs [68, 69], 2D PhCs [70-75], and metamaterials with more aggressive structures [76–79] have been studied. An interesting work by Cao et al. reported a metamaterial emitter that is capable of tuning the peak emission wavelength [76]. The emitting surface consists of periodic gold squares, while the substrate uses a phase-changing material (PCM) made of Ge₂Sb₁Te₄. By switching the PCM (using optical or electrical pulses) between amorphous and crystalline, the peak can be adjusted from $\sim 2.25 \,\mu m$ with emissivity of $\varepsilon_{peak} \sim 0.95$ to $\sim 2.45\,\mu\mathrm{m}$ with $\varepsilon_{peak} \sim 0.8$. Nonetheless, due to the lack of experimental characterizations for these proposed structures, the experimental optical performance, thermal stability, fabrication feasibility, etc., still require further research. For the same reason, the above emitters are not included in Table 3.

Selective Emitter Materials and Designs for High-Temperature Thermophotovoltaic Applications

Table 3: Experimentally demonstrated selective emitters for TPV systems. Data is extracted from published emissivity or radiance. The wavelength in which emissivity is above 0.5 is defined as in-band radiation range. θ is the angle at which emissivity is measured; λ_c is the cutoff wavelength; λ_{peak} is the peak power density wavelength; ε_{in} is the in-band emissivity; ε_{out} is the out-of-band emissivity; η_{se} is the spectral efficiency; M_{in} is the in-band radiance; T is the emitter temperature used in calculation; λ_g is the PV cell bandgap; η_{sys} is the overall (input-energy-to-electricity) system efficiency.

Emitter	Year	Туре	θ ¹	λ _c	λ _{peak} [μm]	ε_{in} [1]	ϵ_{out} [1]	η_e [1]	M_{in} [W/cm ²]	T [K]	Stability	System	λ _g [μm]	η_{sys}^{2} [%]	Fabrication Technique 5
A [33]	1995	Er-Ho doped YAG	N	1.66	1.57	0.46	0.27	0.25	2.10	1500	-	-	-	-	Czochralski method
B [33]	1995	Ho doped YAG	N	2.10	2.07	0.31	0.17	0.43	2.45	1477	-	-	-	-	Czochralski method
C [35]	2000	Al ₂ O ₃ / Er ₃ Al ₅ O ₁₂ composite	N	1.68	1.55	0.52	0.38	0.34	7.97	1780	-	STPV GaSb	1.80	0.02 (550K) ⁴	Bridgman method
D [37]	2001	NiO doped MgO	-	1.75	1.42	0.77	0.24	0.54	9.01	1677	1677K under air-propane flame (working condition)	-	-		Tape-cast doping
E [38]	2002	Er ₂ O ₃ mantle	-	1.58	1.55	0.30	0.18	0.28	2.64	1680	-	-	-	-	-
F [38]	2002	Yb ₂ O ₃ mantle	-	1.06	0.98	0.53	0.13	0.16	1.18	1735	-	-	-	-	-
G [39]	2003	W 2D PhC	N	1.73	1.51	0.81	0.10	0.58	2.55	1400	1h at 1400K in reducing atmosphere hardly changed	-	-	-	EL, FAB etching
H [43]	2011	W 2D PhC	-	2.10	1.64	0.73	0.36	0.31	1.69	1230 ³	-	-	-	-	EL, IL, RIE
I [44]	2012	Ta 2D PhC	N	2.01	1.91	0.79	0.12	0.52	1.32	1200 ³	-	-	-	-	IL, RIE
J [45]	2012	W 2D PhC	N	2.16	1.88	0.77	0.23	0.45	1.94	1230	10h at 1200K in vacuum hardly changed	-	-	-	IL, RIE
K [50]	2013	W-HfO ₂ 3D PhC	-	2.50	1.61	0.89	0.47	0.67	20.27	1673 (1173) ³	1h at 1673K in vacuum some degradation	-	-	-	ALD, RIE
L [50]	2013	HfB ₂ 3D PhC	-	1.54	2.21	0.55	0.45	0.07	0.49	1273 ³	12h at 1273K in vacuum found cracks	-	-	-	CVD, RIE
M [48]	2013	Si-SiO ₂ 1D PhC	N	2.45	2.01	0.64	0.33	0.47	3.16	1293	-	TPV InGaAsSb	2.25	2.50 (1073K) ⁴	LP-CVD, PE-CVD
N [49]	2013	Ta 2D PhC	N	2.07	1.80	0.83	0.28	0.36	1.60	1205	144h at 1173K in vacuum hardly changed	-	-	-	IL, RIE, ALD
O [51]	2014	Si-SiO ₂ 1D PhC	-	2.42	2.18	0.88	0.39	0.49	4.02	1285	-	STPV InGaAsSb	2.25	3.20	LP-CVD, PE-CVD, sputtering

P [52]	2014	Ta 2D PhC	N	2.02	1.81	0.83	0.47	0.29	2.54	1300 ³	-	TPV InGaAsSb	2.30	3.74	IL, RIE, ALD
Q [53]	2015	Si-SiO ₂ -Pt 3D PhC	N	2.50	2.69	0.89	0.26	0.49	1.60	939	8h at 1100K in N2 hardly changed	-	-	-	HF etching, ALD
R [54]	2015	W YSZ-ARC	-	1.94	1.50	0.83	0.19	0.67	10.66	1640 ³	-	STPV GaSb	1.85	8.00	PLD, RF-sputtering
S [55]	2015	W Si ₃ N ₄ -ARC	-	1.60	1.47	0.66	0.09	0.52	2.15	1458 ³	-	STPV GaSb	1.85	6.20	PECVD
T [56]	2016	Mo-HfO ₂ multilayer stack	Н	1.53	1.30	0.75	0.12	0.56	5.02	1640 ³	-	STPV GaSb	1.85	5.10	-
U [57]	2017	Ta 2D PhC	N	2.06	1.75	0.85	0.12	0.65	3.17	1327 3	100h at 1173K in vacuum hardly changed	TPV InGaAsSb	2.00	4.40	IL, RIE, PECVD, e-beam evaporation, ALD
V [58]	2018	W-Al ₂ O ₃ 2D metasurface	N	2.25	1.72	0.76	0.37	0.52	7.02	1473 ³	10 thermal cycles in vacuum at 1473K some degradation	-	-	-	DC-sputtering, ALD, EL, RIE
W [59]	2018	W-CNT 2D PhC	N	1.84	1.61	0.76	0.20	0.36	1.45	1273 ³	168h at 1273K in vacuum negligible degradation	-	-	-	e-beam evaporation, EL, CVD, ALD, RF plasma dry etching
X [60]	2019	W-HfO ₂ 1D metamaterial	N	1.80	1.48	0.76	0.16	0.65	9.32	1673 ³	6h at 1673K in vacuum some degradation	-	-	-	RF-sputtering, DC-sputtering
Y [61]	2019	W-Al ₂ O ₃ 1D metamaterial	N	1.94	1.59	0.81	0.16	0.62	5.21	1473 ³	3h at 1473K in vacuum some degradation	-	-	-	Magnetron sputtering
Z [62]	2020	W-Si ₃ N ₄ multilayer stacks	-	2.18	1.61	0.75	0.19	0.74	13.85	1676 ³	-	STPV GaSb	1.72	8.40	PECVD, DC-sputtering

¹ Angle at which the emissivity is measured. N stands for normal, H stands for hemispherical average, dash stands for unspecified.

² The system efficiencies are obtained from different demonstration setups and contributed by all sources of loss. Therefore, η_{sys} is not recommended as an indicator of the emitter's performance.

 ³ Emissivity is measured at room temperature (or the temperature in parentheses).
 4 The system efficiency is measured at the temperature in parentheses, different from which the emissivity is measured at.

⁵ Abbreviations stand for: e-beam lithography (EL), fast atom beam (FAB) etching, interference lithography (IL), reactive ion etching (RIE), atomic layer deposition (ALD), chemical vapor deposition (CVD), low pressure chemical vapor deposition (LP-CVD), plasma enhanced chemical vapor deposition (PE-CVD), hydrofluoric (HF) etching, radio frequency (RF) sputtering, direct current (DC) sputtering

4. Highly Selective Filters

Another method to pursue high spectral efficiency, in addition to selective thermal emitters, is selective filtering, or cold side spectral control (CSSC). CSSC methods are differentiated from hot side spectral control methods (i.e. selective emitters) by the fact that they are not in physical contact with the emitter, and are therefore maintained at relatively low temperatures. This simplifies the system design by removing two shortcomings most selective emitters suffer from; namely temperature dependent emissivity and degradation at high temperatures. As mentioned previously, the two loss mechanisms in spectral efficiency are absorption of out-of-band (OOB) photons and thermalization of high-energy in-band photons. We will first discuss absorption of out-of-band (OOB) photons and strategies to mitigate these losses.

CSSC methods can be divided into two categories: front surface filters (FSFs) and backside reflectors (BSRs). Backside reflectors provide spectral control by allowing the photodiode to absorb in-band photons (band edge filtering [80]), and reflecting the out-of-band (OOB) photons back to the emitter, commonly known as cold side photon recycling[80]. Since the in-band photons are absorbed by the photodiode, the BSR only needs to have high reflectance for OOB photons and band-gap photons generated by the cell to due radiative recombination. This makes material selection for BSRs less stringent. Metals are commonly used as back surface reflectors for TPV cells since they serve the dual purpose of charge collection and reflection of OOB photons. Swanson [81] used a Si TPV cell with a Ag back reflector, and a 2300 K emitter, to achieve an OOB reflectance of 91%. While Ag is a popular back reflector in solar PV cells due to its high conductivity and reflectance in the visible regime, Au has the best reflectance in the range of 1-10 µm and is a better choice as a BSR for TPV cells.

Using only a Au BSR, and band edge filtering, an OOB reflectance (R_{out}) of 94.5% [82] was achieved with an In-GaAs cell and emitter at 1500 K. Addition of a dielectric spacer between the cell and the Au BSR increased R_{out} an additional 1% to 95.7%. A related work using only a Au BSR achieved an R_{out} of 94.6% [14] using an InGaAs cell and a emitter at 1480 K. The highest R_{out} as of the writing of this review is 99% [15], achieved using an air-bridge architecture with a Au BSR. The air bridge increases R_{out} by eliminating the absorption that takes place at the InP/Au interface, approximately 5% per reflection, giving a radiation-to-electricity efficiency of ~31% with an emitter temperature of 1455 K and an InGaAs cell.

While BSRs are integrated into the TPV cell itself, front surface filters can be mounted on top of the TPV cell, or merely between the emitter and the cell, separating the spectrum control mechanism from the TPV diode and simplifying system design. Unlike BSRs, which require no transmittance and only need to be reflective for OOB photons, the design criteria for a high performance FSF is more stringent. An FSF must be 1) transparent to in-band photons 2) reflective to OOB photons and 3) have extremely low absorption (extinction coefficient less than 0.0001 [83]) over a spectral

range from 1 µm to more than 10 µm.

Front side filters are typically grouped into 1) interference filters 2) plasma filters and 3) tandem filters. Tandem filters are not a standalone category, but a combination of the aforementioned filters, and will be addressed separately to evaluate synergistic effects.

Interference filters, periodic or otherwise, rely on Fresnel reflectance, due to dissimilar refractive indices, and constructive and destructive interference to selectively reflect and transmit the desired wavelengths. The most common interference filter used in TPV systems is a planar, single [82] or multi-layer [84], dielectric stack acting as an antireflection (AR) coating. While most literature does not characterize this as a form of spectral control, and therefore do not measure its individual contribution, it can have a significant effect on system performance. For a single dielectric film, spectral efficiency and power density improvements of 1.7% and 49%, respectively, were observed [82], compared to the case of a Au BSR only. Interference filters are not only applicable to TPV and methods to fabricate them are well understood. While interference filters typically have very low absorption, their effect is dependent on the optical path length; OPL = ns, where n is the refractive index and s is the geometric length. Since OPL is dependent on the angle of incidence, it requires an optimization over all angles of incidence, adding to design complexity.

Plasma filters rely on the collective oscillation of free electrons to reflect light below the plasma frequency (metallike) and transmit light above the plasma frequency (dielectriclike). This mechanism of reflection/transmission, found in metals like silver and gold, can also be found in heavily doped semiconductors and semiconductor oxides (i.e. ITO). The plasma frequencies of metals and transparent conductive oxides (TCOs) are typically too high for TPV applications. Ehsani et al. [85] successfully fabricated heavily doped Si plasma filters for TPV systems, utilizing two different methods to introduce dopants, achieving plasma frequencies in the range of 2-4 µm. Plasma filters using Te doped InPAs have also been grown epitaxially, via metalorganic chemical vapor deposition (MOCVD), with plasma frequencies around 5 µm [86]. While plasma filters theoretically should have high spectral selectivity and good OOB reflectance, they suffer from non-negligible in-band reflectance. This poor in-band performance is why plasma filters are usually paired with another filter in a tandem configuration.

Tandem filters for TPV applications most commonly contain a interference filter and a plasma filter. The interference filter has low in-band reflectance and a sharp wavelength cutoff while the plasma filter has high reflectance at longer wavelengths where interference filters fall short; see Fig. 11. The most widely used type of tandem filter features an interference filter, using a combination of $\mathrm{Sb}_2\mathrm{Se}_3$ (n=3.4) and YF_3 (n=1.5), on top of an n-doped InPAs plasma filter [83, 84, 86–88]. This tandem filter when paired with In-GaAs/InPAs diodes and a SiC graybody emitter at $1058^{\circ}\mathrm{C}$, achieved a spectral efficiency of $\sim 60\%$ [84]. When paired with a $0.52~\mathrm{eV}$ or $0.60~\mathrm{eV}$ diode and a $950^{\circ}\mathrm{C}$ emitter, Four-

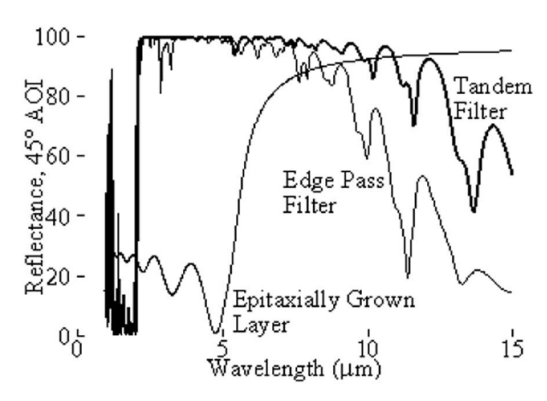


Figure 11: Tandem filter performance at 45° angle of incidence, showing component reflectances of tandem and plasma filters. Reprinted with permission from [83] \bigcirc The Optical Society

spring et al. [83] achieved a spectral efficiency of 75-80%. Yeng et al.[87], using a 1320 K selective emitter, optimized tandem filter, and InGaAs cell, achieved 25% radiation-to-electricity efficiency. They predicted that an ideal cell with the same spectral efficiency could reach 45.7% radiation-to-electricity efficiency with an identical spectral control scheme. Crowley et al. [88] looked into using TPV for radioisotope power systems (RPS), using an InGaAs cell and 1350 K graphite emitter and tandem filter. They achieved 19% radiation-to-electricity efficiency and 80% calculated spectral efficiency.

The second loss mechanism for spectral efficiency is thermalization of high energy photons. These losses can be minimized by a few different methods. The first method is to increase the cell bandgap for a given emitter temperature; increasing E_{α} in Eq. 3. For an ideal filter, BSR or FSF, this would simply change the ratio of OOB to in-band photons, decreasing power density while increasing efficiency. But the non-unity reflectivity of a real filter will determine the ideal cell bandgap for a given emitter temperature [14]. Use of multi-junction TPV cells decreases thermalization losses, similarly to increasing the cell bandgap, but don't suffer the loss in efficiency since additional cells utilize what would have been recycled as OOB photons [89]. Multi-junction cells also benefit from lower resistive losses since each individual cell operates at a lower current density. The final method for reducing thermalization losses is to reduce the intensity of the high energy photons interacting with the cell. This can be achieved by use of narrow-band, instead of broad-band, emitters; see Figure 6. Filter designs whose goal is to recycle the high energy photons is an area of research that has yet to be explored, probably because thermalization of high energy photons is the non-dominant loss mechanism for spectral efficiency.

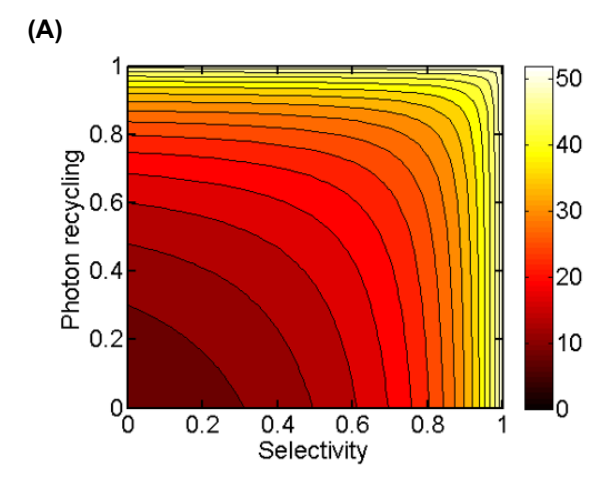
TPV systems that focus on the back surface reflector have seen the largest improvement in performance over the last couple years, with the record radiation-to-electricity efficiency air-bridge structure being published in September of 2020. Front surface filters have seen few papers published in the last decade. We attribute this to 1) the more stringent per-

formance requirements for front surface filters compared to back surface reflectors and 2) a lack of novel FSF designs. What is interesting when comparing BSRs and FSFs, is that the best FSF spectral efficiency (~ 80%)[83, 86] is higher than the best BSR spectral efficiency (71.4%) [15]. FSFs also remove the need for OOB spectral selectivity from the TPV cell, eliminating any concerns over sub-bandgap absorption, and making the cell solely responsible for in-band absorption. Considering that most of the FSF papers were published before 2006, and that the more recent BSR papers benefited from a decade and half of advances in TPV diode research and fabrication, FSFs might be worth another look; more than likely paired with a high performing BSR.

5. Trade-offs and Interactions between Thermal Emitters and Filters

To understand the trade-offs and interactions between thermal emitters and filters, it is possible to create a simple model for the TPV efficiency, following the fundamental tenets of TPV operation outlined in Section 2, above. In this model, the view factor can be assumed to be 1, the PV bandgap can be fixed at 0.74 eV, dark current can be taken at a nominal value of 1.1 nA/cm², the input power to the PV cell can be assumed to be 20 W/cm², and the emitter temperature taken to be 1573 K. If we define selectivity as the relative suppression of below-bandgap emissivity for the emitter, and define photon recycling efficiency as the fraction of photons below bandgap that are returned to the emitter, the TPV efficiency results can be seen in Fig. 12. It is evident that the efficiency even under favorable conditions can be quite low in the absence of either photon recycling or selectivity, but it also increases considerably as either of these metrics increases. Note that while the effects of selectivity and recycling are symmetric, the combined performance exceeds that of one of the metrics alone. (This result appears to differ from that of [14], but it can be understood as follows: [14] considers the asymptotic case where both r and R are close to unity, in which case all parasitic losses are fairly low, whereas this analysis considers a fuller range of values, and calculates the full system efficiency, instead of just the parasitic losses.) This analysis suggests that combining both approaches should yield optimal results. For instance, combining the record 30% air-bridge filter design with a slightly selective heat source could yield even higher performance. However, if there are any experimental constraints on combining the two approaches, it may change this analysis.

Next, we consider the trade-off between selectivity and recycling in the case where the efficacy of recycling is more limited - for instance, when the heat source is distant enough that the effective view factor is small - such as solar TPV; Fig. 12. In this case, photon recycling does not improve the efficiency of collecting solar photons, so a minimum level of selectivity is required in the filter to obtain non-zero efficiencies. In this scenario, it can be seen that selectivity is preferred to recycling. Nonetheless, the presence of recycling does improve the efficiency of even fairly selective



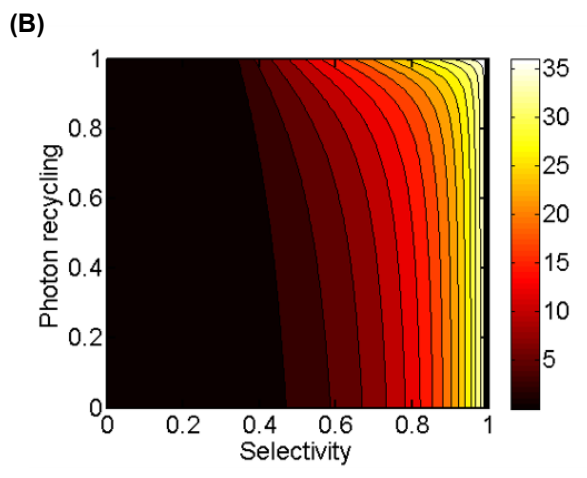


Figure 12: (A) TPV efficiency and (B) Solar TPV efficiency in an emitter-filter-PV design, as a function of photon recycling efficiency(i.e., the probability of below bandgap photons returning to the emitter) and selectivity (i.e., the relative suppression of below-bandgap emissivity for the emitter). Increasing both metrics has a significant benefit for TPV efficiency. In (B), note that the additional losses associated with capturing sunlight as heat limits the efficacy of photon recycling.

structures, so it is still valuable in this scenario.

For most lab scale experiments, view factors are significantly less than unity and optimizing the TPV cell layer thicknesses for maximum absorption at wavelengths above the cell bandgap, and across the applicable angles of incidence, is vital for high power density and efficiency. And while significant improvements in performance have been made in these low view factor systems, these gains don't directly translate to performance at high view factors; when a TPV design is scaled up. Low view factor systems are primarily concerned with incident angles from zero to a few tens of degrees, while an infinite flat plate Lambertian emitter, with a view factor of unity, reaches the peak of its angular distribution of incident photons at 45° following a $\sin \theta \cos \theta$ relationship [90]. These higher view factors provide greater potential for photon recycling, and less stringent requirements on the emitter selectivity.

The overall takeaway from this analysis is that while se-

lectivity and photon recycling can both improve TPV system efficiencies, selectivity is more important in situations involving low view factors, while photon recycling is about equally effective in high view factor situations.

6. Materials Thermal Stability

6.1. Structures and Materials

Optical spectral selectivity is enabled by materials or structures that can selectively absorb or transmit desirable light, and reflect unused light. Some transition metals [37, 91] and rare earth oxides [38, 92] exhibit capability to selectively emit light. However, those intrinsically selective materials cannot provide tunability of the emission cutoff energy. Selective peak wavelength is linked to the atomic structure of the materials and cannot be shifted easily [93]. Thus, photonic crystals (PhCs) are more commonly used as selective emitters. Understanding the thermal properties of materials is crucial for further improving the thermal stability of selective emitters. Here, a discussion of the thermal-related-properties of materials in PhCs is provided.

PhCs usually have a periodic stack of metals and oxides. As summarized in Table 2, Si, W, Ta, Pt and Mo are commonly used metals in PhCs. However, the non-refractory materials such as Si or Pt with low melting temperatures limit high-temperature stability of the emitter designs. Therefore, PhCs using refractory metals (W, Mo, Ta) as the absorber/emitter materials are more promising to achieve hightemperature stability. Although refractory metals have a high melting temperature (Table 4), one challenge of refractory metals is that they are easily oxidized during high-temperature annealing. A detailed discussion of metal oxidation is provided in section 6.2.1. A stable oxide "cap" layer can help in preventing oxygen diffusion into metal layers. [94] Refractive oxides (HfO2, Al2O3, etc) are also widely used in 1D PhCs as dialectic spacer or protective layer. Besides melting points, thermal expansion coefficient (CTE) is another key parameter when considering thermal stability. Annealing PhCs containing materials with distinct CTE can also result in structure degradation, which will be discussed in detail in section 6.2.4. Table 4 summarizes thermal-relatedproperties of the commonly used or possible candidate refractory materials in high-temperature PhCs, which can help in searching for new material combinations.

Besides the structural and thermal properties of metals and oxides, the fabrication technique is another issue to be considered regarding the emitter stability. Table 3 summarizes the corresponding techniques for bulk and PhC emitters. Liquid-solid processes, including Czochralski and Bridgman methods [33, 35], were used extensively for bulk emitter fabrication. These processes are widely adopted in the industry to produce monocrystal, due to their low cost and relatively high growth rate. Since 1D PhCs usually have a periodic multilayer stack of alternating metal and oxide layers, RF- or DC- sputtering, [54, 58, 60] low-pressure chemical vapor deposition (LPCVD) or plasma-enhanced chemical vapor deposition (PECVD) [55, 57, 62], and atomic layer

deposition (ALD) [49, 50, 52, 53, 58] are more common techniques for multilayer structures. These deposition techniques can achieve good thickness control and reasonable film crystallinity compared to liquid-solid processes. A vacuum environment is desired for conformal surface coating. On the other hand, 2D and 3D PhCs require a more complicated fabrication process due to their metasurface or nanocavities design. Lithography (e-beam lithography (EL), interference lithography (IL)) [39, 43-45] and etching (reactive ion etching (RIE) or fast atom beam (FAB) etching) [39, 43– 45] were first applied to define the PhC patterns (e.g. arrays, microcavities) on the substrates. Deposition techniques similar to 1D PhCs, i.e, CVD, sputtering, ALD, and PLD, are then used to fabricate multilayer structure or protective coatings. Refractory metals and oxides are widely adopted in the PhC designs. However, high-temperature stability could still be a concern as Si and SiO2 are used in the systems. The concerns on oxidation of the refractory metals, e.g., W, remain in these designs. More details of these failure mechanisms are discussed below.

6.2. Failure Mechanisms and Their Mitigation Approaches

Structured selective emitters often suffer from high temperature degradation during operation due to the increased kinetic energy of atoms under elevated temperatures. According to numerical studies [97, 98] as well as experimental demonstrations, [60, 61, 99–104] high temperature stability of structured selective emitters is usually limited by several failure mechanisms including oxidation, grain coarsening, surface diffusion, and thermal expansion. In this section, these failure mechanisms are discussed from a material science aspect, and their mitigation approaches are also discussed.

6.2.1. Oxidation

Under low and medium vacuum conditions, the key failure mechanism is metal oxidation. [99] The source of oxygen may come from an external environment or adjacent oxide layers. Refractory oxides (HfO2, Al2O3, etc.) are usually more thermodynamically stable than metal-formed oxides (WOx, MoOx, etc.). As summarised in Table 4, the free enthalpy of the formation of refractory oxides is smaller than that of metal-formed oxides, which suggests oxygen atoms are more likely to remain in the oxide layers. Therefore, the interlayer diffusion of oxygen from adjacent refractory oxide to metal could be neglected [60, 61] Compared to interlayer diffusion, external oxygen diffusion via grain boundaries dominates the degradation of structured emitter. Figure 12(a) shows the metal layer close to the surface contains more oxygen than the layer close to the substrate, which is evidence of external oxygen. [60] In order to improve film quality and reduce grain boundaries, selecting two materials with similar lattice structures would be helpful.

Since oxidation is one of the most common degradation mechanisms observed in selective emitters, several approaches have been demonstrated to mitigate the oxygen diffusion either from external environment or from adjacent oxide. Intuitively, high vacuum (e.g. below 10^{-5} mbar) and inert gas (e.g. Ar) atmospheres can effectively reduce the oxygen from the external environment [60, 100]. Since the oxygen will diffuse into the emitter structure and potentially react with the refractory metals, high vacuum packaging can effectively minimize the residual oxygen in the chamber. On the other hand, an inert gas atmosphere is likely to be a more economically feasible approach for long-term TPV packaging. Both approaches demonstrate the thermal stability for W-HfO₂ structure up to 1400°C over 6 hrs (Table 5) [60, 100].

For oxygen diffusion through the adjacent layers, a stable protective coating can prevent oxidation [50, 97, 105]. Although many refractory materials (TiN, W, Au, SrRuO₃, etc.) can withstand high temperatures, reliability is a major concern for materials selection. As a result, TiN and HfO₂ are selected as two common diffusion barriers in emitter designs, because their optical properties are retained after multiple thermal cycles and these protective coating will not interfere with the emission spectrum. As summarized in Table 5, a HfO₂ protective coating enabled the emitter to operate at 1000°C for at least 12 hrs [50].

6.2.2. Grain Growth and Recrystallization

By operating under high vacuum conditions, oxygen from the external environment becomes less important in high temperature degradation. Instead, void and metal agglomeration are frequently observed after high vacuum annealing. Voids occur because of grain growth [60], phase transition [101], and sublimation [100] under high temperatures. According to Mullins et al. [106], the diffusion is proportional to second derivative of the curvature. Once some non-flat area occurs in the metal layers, the metal structures tend to form round particles by grain boundary- and interface- diffusion to reduce the overall surface energy (Fig.13(b)).

For practical TPV applications, polycrystalline substrates are more commercially available than single crystal substrates. By definition, polycrystalline substrates tend to have much smaller grain sizes than single crystals. These small grains are also less thermodynamically stable compared to their single crystal counterparts, which can interfere with the aforementioned PhC patterns of similar size. The degradation is attributed to two factors: low melting point and strain relaxation [49, 65]. On one hand, polycrystalline substrates typically have much lower melting points compared to single crystal substrates, and grain boundary migration at high temperature could disintegrate the PhC structure. Additionally, the internal stress stored during TPV fabrication will be released under elevated temperature, and grains will thus nucleate and grow at TPV operating temperatures [97]. To avoid the degradation from grain growth and recrystallization, polycrystalline substrates are pre-annealed at an elevated temperature for a prolonged time. The pre-annealing process gives rise to large grains and less grain boundaries, which presents a notable increase in high-temperature structural stability. Hence, pre-annealing is potentially a low-cost

Table 4
Structure and Thermal Properties of Refractory Metals and Oxides

		1				
	Refractory Material	Melting Temperature [°C]	Thermal Expansion Coefficienct $\times 10^{-6} [\mathrm{K}^{-1}][95]$	Structure and Lattice Parameter $[\mathring{A}]$ Unit cell defined by a, b, c and α , β , γ	Free enthalpy for the formation at 1400 K [kJ mol ⁻¹][96]	
	W	3422	4.31	Cubic a=3.165	WO ₂ : -574.467 WO (volatile): -821.253	
Metals	Мо	2623	5.35	Cubic a=3.147	MoO ₂ : -571.569 MoO ₃ (volatile): -667.350	
	Та	3017	6.64	Cubic a=3.303	Ta ₂ O ₅ : -2007.797	
	MgO	2852	11.52	Cubic a=4.20	-735.143	
	HfO ₂	2900	5.85	Monoclinic a=5.116 b=5.172 c=5.295	-1130.175	
	α -Al ₂ O ₃	2054	7.1-8.3	Trigonal a=4.759 c=12.98	-1689.189	
	α -SiO $_2$	1710	0.55	Trigonal a=4.913 c=5.405	-899.810	
	ZrO ₂	2710	7.56	Monoclinic a=5.146 b=5.207 c=5.311	-1089.866	
Oxides	TiO ₂	1855	7.14	Tetragonal a=4.594 c=2.962	-939.729	
	CeO ₂	2340	10.6	Cubic a=5.411	-1088.399	
	Eu ₂ O ₃	2350	7.02	Cubic a=9.504	-1651.778	
	BeO	2550-2565	7.5-9.7	Trigonal a=2.70 c=4.39	-605.181	
	CaO	2927	3.88	Cubic a=4.811	-640.850	
	Cr ₂ O ₃	2330	10.9	Trigonal $a=5.38$ $\alpha = 54°50'$	-1126.195	
	Y ₂ O ₃ 2439 8.10		8.10	Trigonal a=3.688 c=5.919	-1890.448	

approach for large-scale TPV fabrication [49, 65, 97].

Apart from pre-annealing, alloying can also be considered as a practical approach for hindering undesirable grain growth in 3D inverse opals. Doping tungsten with 3 wt% molybdenum can effectively slow down the grain coarsening and dislocation diffusion, and the thermal stability temperature range can be improved by at least 200°C [107].

6.2.3. Surface Diffusion

As mentioned above, the diffusion is proportional to second derivative of the curvature. Diffusion on an ideal flat surface is zero, and results in no structural changes. On the other hand, diffusion on a curved surface will lead to changes in the structure. Thus, 2D and 3D structures contain more curvature, with sharp edges strongly suppressed by surface diffusion [97–99, 102]. Fig.13(c) shows an example of the structural degradation of the 2D microcavity structure.

The surface diffusion can be a dominant degradation factor for curved surfaces and nanostructured designs (e.g. inverse opals). Initially, since the surface diffusion is proportional to the curvature, it is intuitively obvious to design a geometrically flat (zero curvature) surface to avoid curvature dependent structural degradation. This structure can be fabricated by plugging the patterned surface cavities with an

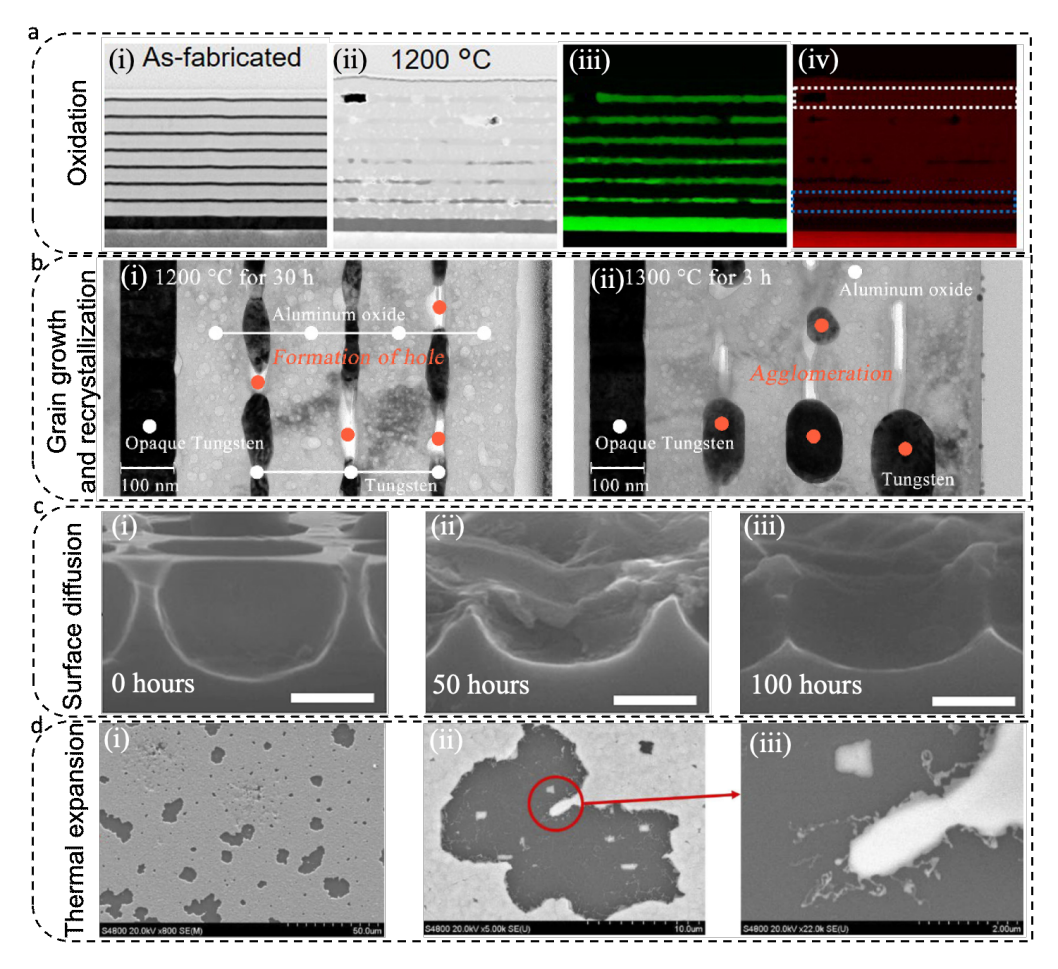


Figure 13: Failure mechanisms of structured selective emitters. a) Oxidation. STEM image (i) for as-fabricated layered metamaterial emitter. STEM image (ii), W element mapping (iii), and O element mapping (iv) for annealed emitter [60] b) Grain growth and recrystallization. Cross section of the metamaterial samples after exposed to 1200 °C for 30 h (i) and 1300 °C for 3 h (ii). Reprinted with permission from [61] © The Optical Society c) Surface diffusion. SEM cross-section images of Si microcavities after 0 h (i), 50 h (ii), and 100 h (iii) of firing at 673 K. Reprinted from [97], with the permission of AIP Publishing d) Thermal expansion. SEM images (i) and zoom in area (ii) (iii) after 24 h thermal stability test. Reprinted with permission from [103] © The Optical Society

oxide ceramic (e.g. HfO₂) [97]. In order to maintain selective emission and to avoid cracking, the ceramic plugs should have both IR transparency and compatible thermal expansion with the substrate. Another approach to retard the surface diffusion is by morphology design and spatial separation [60, 98]. According to the simulation, the lower curvature and its derivative caused by large cavity sidewalls (i.e., increasing the periods and decreasing cavity widths) will significantly reduce the surface diffusion rate. As a result, HfO₂-plugged microcavities provided a long lifetime for W emitters operating at 827°C [97], and spatially confined edgeless W layers exhibited no obvious degradation up to 1400°C over 6 hrs [60, 98] (Table 5).

If thermal stability is dominated by the surface-to-volume ratio at the interface, which is common in 3D nanostructured designs, surface diffusion can be effectively mitigated by a protective coating [49, 97, 99, 108]. Specifically, these thin ceramic layers can impede the surface diffusion and pre-

vent the structural degradation caused by sintering and grain coarsening. The structural integrity can thus be retained at high temperatures. As summarized in Table 5, a 20 nm HfO_2 protective layer on 2D Ta PhC observed no degradation at 900°C for at least 144 hrs [49], and the HfO₂ coating on W inverse opals enabled the emitter to operate at 1400°C for at least 12 hrs [97].

6.2.4. Thermal Expansion

Structure degradation often occurs after high temperature annealing because of the mismatch of the coefficient of linear thermal expansion (CTE) between adjacent materials [103, 104]. The CTE of materials is defined as:

$$CTE = \frac{\epsilon}{\Delta T} = \frac{\Delta l}{l \times \Delta T},\tag{7}$$

where ϵ is the relative increase in length, ΔT is the temperature change, Δl is the length change, and l is the particular length measurement. When heating at a given tem-

Failure Mechanism	Mitigation Approaches	Temperature [°C]	Stability	Environment	Emitters	Comments
Oxidation	High vacuum [60]	1400	Over 6h	High Vacuum 3×10^{-5} bar	W-HfO2 1D metamaterial	Experiment
	Inert gas atmosphere [100]	1300	6h	Ar	W-HfO2 1D multilayer	Experiment
	HfO ₂ protective coating [50]	1400	1h	Ar	W-HfO2 3D PhC	Experiment
	Pre-annealing [97]	900	22h	*	W-HfO2 3D PhC	Experiment
Grain Growth &	Pre-annealing [65]	910	1 week	*	Ta 2D PhC	Experiment
Recrystallization	Pre-annealing [49]	900	144h	100 mTorr Ar	Ta 2D PhC	Experiment
	Alloying [107]	800	4h	0.5L/min N_2	WMo 3D PhC	Experiment
	Hf-plugged microcavities [97]	900	22h	*	W 2D PhC	Experiment
	Passivation Layer [99]	1400	12h	5% H ₂ in Ar	W-HfO2 3D PhC	Experiment
	Morphology Design [98]	927	1000h	*	Ta 1D PhC	Simulation
Surface Diffusion	Morphology design [60]	1400	Over 6h	High Vacuum 3×10^{-5} bar	W-HfO2 1D metamaterial	Experiment
	Protective Coating [49]	900	144h	100 mTorr Ar	Ta 2D PhC	Experiment
	HfO ₂ coating [108]	1200	176h	*	W-HfO2 2D PhC	Experiment
Thermal Expansion	Thick Ta Coating [109]	1100	1h	Vacuum	Ta-HfO2 1D PhC	Experiment

 Table 5

 Failure Mechanisms and Mitigation Approaches

perature, materials with different CTE values would tend to expand by different amounts. These differences in elongation lead to thermomechanical stress between adjacent materials, which may further cause the layers to yield and delaminate (Fig.13(d)). Hence, this thermally-induced delamination can become severe as the operating temperature increases.

In order to avoid cracking and debonding of the structure, the functional layers should be thermo-mechanically compatible with the substrate, i.e., the CTE of the functional layers should be comparable to or larger than that of the substrate. As a result, the functional layer expands more than the substrate at the elevated temperature, and the consequent compressive stress across the interface will mechanically secure the whole structure. [97, 109] A summary of CTE of refractory metals and oxides is provided in Table 4, which can help in choosing functional layers and substrates.

7. Challenges

Although researchers have made significant progress in TPV performance, there are still many obstacles impeding TPV technologies from large-scale implementation. Scalability and fabrication cost are probably the two major factors. For high-performance 2D/3D PhC selective emitters (most popular in recent works), the fabrication techniques usually involve lithography, PVD/CVD, etching, etc. This can be rather expensive, time-consuming, and low-yield, making large-scale fabrication impractical. Bulk and 1D PhC emitters usually do not require lithography and etching, nonetheless, PVD/CVD is needed for material growth. Rare-earth composite emitters are most likely to achieve large-scale fabrication, however, typically have a low spectral efficiency,

low in-band radiance, and are mechanically fragile. Rare-earth doped YAG, on the other hand, is both chemically and mechanically stable but still faces similar issues as composite emitters. Plus, YAG is a very expensive material which can cost above ~\$50/cm² (1 mm thick) according to the most recent commercial prices (e.g., EKSMA Optics, Newlight Photonics).

Low efficiency is another issue for current TPV/STPV systems. The highest system efficiency reported by far is still stuck below 10%, whereas the competing technologies such as flat-panel photovoltaics (PV), concentrating photovoltaics (CPV), and concentrating solar power (CSP) can easily reach 20~30% in a large-scale and low-cost manner (e.g., Cheetah from JinkoSolar, uModuleTM from ArzonSolar, Stirling Energy Systems from Sandia National Laboratories). Fossil fuel power plants equipped with ultra-supercritical steam turbines (e.g., Siemens SST-6000) can even achieve net plant efficiency above 45% (fuel energy to electricity supplied to the grid, plant overhead power consumption considered), which are still the major source of global electricity, contributing more than 60% of the total generated power. TPV/STPV serve the same purpose of converting solar, fuel, or other heat sources to electricity, yet are not comparable to any of the above methods at present. Although the theoretical efficiency of TPV can be relatively high thanks to the perfect spectrum match, the multistep energy conversion (see Fig.2) introduces energy loss at each stage and quickly results in poor performance in real case. Not only the selective emitter is crucial, the whole system, including combustor, solar absorber and concentrator, vacuum cavity, low-bandgap PV cell, etc., needs to be carefully designed to ensure the overall efficiency.

Another challenge of TPV is the high operating temper-

^{*} Environment not specified in original publication

ature induced reliability issues. Complex structures such as high vacuum environment is usually a must-have to prevent emitter degradation, which inevitably increases the cost and reduces the overall mechanical robustness. In addition, the high operating temperature also limits the application scenarios. Stirling engines and thermoelectric generators can operate at temperatures as low as ~100°C with a comparable efficiency to state-of-the-art TPVs (when operating at above 1000°C). They both can be made as a portable device for personal power generation, making them potential competitors against TPV. At higher temperatures (e.g., ~600°C, still far below than TPV), Stirling engines can achieve greater than ~30% thermal efficiency [110–112] without worrying thermal degradation.

The cost, efficiency, and reliability for TPV systems need to be significantly improved before real-world applications.

8. Summary and Future Perspectives

This review aimed to summarize the key issues for selective emitters and filters that affect the performance of TPV systems. As discussed, there are 3 major types of emitters bulk refractory, rare earth, and photonic crystal - all of which are subject to questions about thermal and chemical stability at high temperatures under different atmospheric conditions. Generally, the trend has been that the most robust emitters, bulk refractory materials, exhibit the least selectivity, while the least robust emitters, 3D photonic crystals, exhibit the greatest selectivity. Therefore, improving thermal stability is also key to achieving greater selectivity, efficiency, and long-term performance. In addition, near-field TPV devices, which can in principle transfer more than the far-field Planck distribution through evanescent fields, also require thermal stability and spectral efficiency, but the design details will be different from their more conventional far-field TPV device counterparts.

Considering the current selective emitter designs, most of the thermal stability tests were conducted up to 1400 °C for 12 hours, however with obvious failure observed in most of the cases. Thus, high-temperature stability analysis is needed to successfully reach the operation temperatures required for very high efficiency TPV designs. Temperature-induced failure analysis can be carried out under further elevated temperatures in the range of 1000°C to 1500°C. In this range, materials selections and nanostructure designs are likely to be even more limited than at lower temperatures.

Considering the materials candidates, beyond refractory metals and oxides, high-temperature ceramics, especially oxides and nitrides, with excellent thermal stability and chemical compatibility could be ideal for minimizing interdiffusion, grain growth and interfacial reactions. In addition, for most of the high-temperature ceramics, e.g., oxides and nitrides, their crystal structures and lattice parameters as well as their thermal expansion coefficients are very close. Thus, the integration of these heterostructures could be easier in terms of high-quality thin film growth. The thermal coefficient mismatch could also be minimized and the thermal

stress induced delamination can be mitigated. Table 4 summarize the structure and thermal properties of refractory metals and oxides. Future research in integrating nanostructured oxide/oxide and oxide/nitride heterostructures as selective emitter designs could be a promising direction.

We also discussed two types of filters: front surface filters and backside reflectors. While front surface filters have more stringent performance requirements, they remove the task of spectral control from the TPV cell, simplifying cell design. Back surface reflectors are integrated into the TPV cell and benefit from the intrinsic filtering it provides, lowering the number of system components. Both are acceptable methods to attain high spectral efficiency. Given the recent progress in spectral filtering, future research on increasing in-band emissivity (to increase power density) and/or increasing reflectance of in-band photons with energies high above the bandgap (to improve spectral efficiency and PCE) could be promising.

We then showed that the benefits of filters and emitters are complementary and mutually reinforcing, thus emphasizing the importance of improving both.

The challenges that current TPV systems face are also briefly discussed toward the end, including high fabrication cost, poor scalability, low efficiency, limited application scenarios, and complex structures. These weaknesses bring TPV huge disadvantages over the competing technologies such as PV, CPV, and Stirling engines, hindering it from large-scale applications at the current stage. Much more research needs to be carried out to seek the solutions for the above issues, pushing the TPV performance closer to its theoretical limit.

In future work, we recommend that thermal stability of photonic crystal-based structures receive further attention in TPV research, with emphasis on using combinations of materials with the greatest potential for robust, long-term stability under a range of realistic conditions, which include not only high temperatures but oxidizing atmospheres. Realizing experimentally-fabricable photonic crystal structures with greater inherent resilience is most likely a key path to improved overall TPV efficiency that can complement recent breakthroughs in high-performance filtering.

Credit Authorship Contribution Statement

Peter Bermel and Haiyan Wang -Conceptualization, Funding Acquisition, Project administration; and Writing-original draft and review & editing; **Changkyun Lee, David Kortge, Jiawei Song, Jie Zhu, Ze Wang, and Zihao He** - Data curation, Visualization, Roles/Writing - original draft, and Writing - review & editing.

Declaration of Competing Interest

The authors declare that they have no known competing financial interests or personal relationships that could have appeared to influence the work reported in this paper.

Acknowledgments

We acknowledge support from the Defense Advanced Research Projects Agency [grant number HR00112190006]; PB and ZW acknowledge the National Science Foundation [grants numbers EEC1454315-CAREER, EEC-1227110, CBET-1855882]; and PB and DK acknowledge the Office of Naval Research [grant number N00014-19-S-B001]. The views, opinions and/or findings expressed are those of the authors and should not be interpreted as representing the official views or policies of the Department of Defense or the U.S. Government.

Data Availability

Please contact the original authors cited for the applicable data.

References

- [1] Thomas Bauer. Thermophotovoltaics: basic principles and critical aspects of system design. Springer Science & Business Media, 2011.
- [2] Hoofar Daneshvar, Rajiv Prinja, and Nazir P Kherani. Thermophotovoltaics: Fundamentals, challenges and prospects. <u>Applied Energy</u>, 159:560–575, 2015.
- [3] Sean Molesky and Zubin Jacob. Ideal near-field thermophotovoltaic cells. Physical Review B, 91(20):205435, 2015.
- [4] Zhiguang Zhou, Qingshuang Chen, and Peter Bermel. Prospects for high-performance thermophotovoltaic conversion efficiencies exceeding the shockley–queisser limit. <u>Energy Conversion and Management</u>, 97:63–69, 2015.
- [5] KF Mustafa, S Abdullah, MZ Abdullah, and K Sopian. A review of combustion-driven thermoelectric (te) and thermophotovoltaic (tpv) power systems. <u>Renewable and Sustainable Energy Reviews</u>, 71: 572–584, 2017.
- [6] A Datas and A Martí. Thermophotovoltaic energy in space applications: Review and future potential. <u>Solar Energy Materials and Solar Cells</u>, 161:285–296, 2017.
- [7] Reyu Sakakibara, Veronika Stelmakh, Walker R Chan, Michael Ghebrebrhan, John D Joannopoulos, Marin Soljacic, and Ivan Čelanović. Practical emitters for thermophotovoltaics: a review. <u>Journal of Photonics for Energy</u>, 9(3):032713, 2019.
- [8] Abigail Licht, Nicole Pfiester, Dante DeMeo, John Chivers, and Thomas E Vandervelde. A review of advances in thermophotovoltaics for power generation and waste heat harvesting. <u>MRS</u> <u>Advances</u>, 4(41):2271–2282, 2019.
- [9] Yang Wang, Haizhou Liu, and Jia Zhu. Solar thermophotovoltaics: Progress, challenges, and opportunities. <u>APL Materials</u>, 7(8): 080906, 2019.
- [10] Shiquan Shan, Chuyang Chen, Peter G Loutzenhiser, Devesh Ranjan, Zhijun Zhou, and Zhuomin M Zhang. Spectral emittance measurements of micro/nanostructures in energy conversion: a review. Frontiers in Energy, pages 1–28, 2020.
- [11] Tobias Burger, Caroline Sempere, Bosun Roy-Layinde, and Andrej Lenert. Present efficiencies and future opportunities in thermophotovoltaics. <u>Joule</u>, 2020.
- [12] Xueji Wang, Ryan Starko-Bowes, Chinmay Khandekar, and Zubin Jacob. High-temperature thermal photonics. <u>Annual Review of Heat</u> Transfer, 23, 2020.
- [13] Tobias Burger, Caroline Sempere, and Andrej Lenert. Thermophotovoltaic energy conversion: materials and device engineering. Nanoscale Energy Transport, 2020.
- [14] Zunaid Omair, Gregg Scranton, Luis M Pazos-Outón, T Patrick Xiao, Myles A Steiner, Vidya Ganapati, Per F Peterson, John Holzrichter, Harry Atwater, and Eli Yablonovitch. Ultraefficient thermophotovoltaic power conversion by band-edge spectral filter-

- ing. Proceedings of the National Academy of Sciences, 116(31): 15356–15361, 2019.
- [15] Dejiu Fan, Tobias Burger, Sean McSherry, Byungjun Lee, Andrej Lenert, and Stephen R Forrest. Near-perfect photon utilization in an air-bridge thermophotovoltaic cell. <u>Nature</u>, 586(7828):237–241, 2020
- [16] Alejandro Datas, Alba Ramos, Antonio Martí, Carlos del Cañizo, and Antonio Luque. Ultra high temperature latent heat energy storage and thermophotovoltaic energy conversion. <u>Energy</u>, 107:542– 549, 2016.
- [17] Xianglei Liu, Liping Wang, and Zhuomin M Zhang. Near-field thermal radiation: recent progress and outlook. <u>Nanoscale and</u> Microscale Thermophysical Engineering, 19(2):98–126, 2015.
- [18] Peter Bermel, Michael Ghebrebrhan, Walker Chan, Yi Xiang Yeng, Mohammad Araghchini, Rafif Hamam, Christopher H Marton, Klavs F Jensen, Marin Soljačić, John D Joannopoulos, et al. Design and global optimization of high-efficiency thermophotovoltaic systems. Optics express, 18(103):A314–A334, 2010.
- [19] William Shockley and Hans J Queisser. Detailed balance limit of efficiency of p-n junction solar cells. <u>Journal of applied physics</u>, 32 (3):510–519, 1961.
- [20] Martin A Green. Solar cells: operating principles, technology, and system applications. Englewood Cliffs, 1982.
- [21] G Martinelli and M Stefancich. Solar cell cooling. <u>Springer Series</u> in Optical Sciences, 130:133, 2007.
- [22] IB Bhat, JM Borrego, RJ Gutmann, and AG Ostrogorsky. Tpv energy conversion: a review of material and cell related issues. In IECEC 96. Proceedings of the 31st Intersociety Energy Conversion Engineering Conference, volume 2, pages 968–973. IEEE, 1996.
- [23] PF Baldasaro, JE Raynolds, GW Charache, DM DePoy, CT Ballinger, T Donovan, and JM Borrego. Thermodynamic analysis of thermophotovoltaic efficiency and power density tradeoffs. Journal of Applied Physics, 89(6):3319–3327, 2001.
- [24] Simon M Sze and Kwok K Ng. <u>Physics of semiconductor devices</u>. John wiley & sons, 2007.
- [25] Lewis M Fraas and Larry D Partain. <u>Solar cells and their</u> applications, volume 236. John Wiley & Sons, 2010.
- [26] Robert E Nelson. A brief history of thermophotovoltaic development. Semiconductor Science and Technology, 18(5):S141, 2003.
- [27] Caleb Amy, Hamid Reza Seyf, Myles A Steiner, Daniel J Friedman, and Asegun Henry. Thermal energy grid storage using multi-junction photovoltaics. <u>Energy & Environmental Science</u>, 12(1): 334–343, 2019.
- [28] Zhiguang Zhou, Xingshu Sun, and Peter Bermel. Radiative cooling for thermophotovoltaic systems. In <u>Infrared Remote Sensing and</u> <u>Instrumentation XXIV</u>, volume 9973, page 997308. International Society for Optics and Photonics, 2016.
- [29] Zhiguang Zhou, Ze Wang, and Peter Bermel. Radiative cooling for low-bandgap photovoltaics under concentrated sunlight. <u>Optics</u> <u>express</u>, 27(8):A404–A418, 2019.
- [30] Ze Wang, David Kortge, Jie Zhu, Zhiguang Zhou, Hans Torsina, Changkyun Lee, and Peter Bermel. Lightweight, passive radiative cooling to enhance concentrating photovoltaics. <u>Joule</u>, 4(12):2702– 2717, 2020.
- [31] Roland A Lowe, Donald L Chubb, Serene C Farmer, and Brian S Good. Rare-earth garnet selective emitter. <u>Applied physics letters</u>, 64(26):3551–3553, 1994.
- [32] Udo C Pernisz and Chandan K Saha. Silicon carbide emitter and burner elements for a tpv converter. In <u>AIP Conference Proceedings</u>, volume 321, pages 99–105. American Institute of Physics, 1995.
- [33] Roland A Lowe, Donald L Chubb, and Brian S Good. Radiative performance of rare earth garnet thin film selective emitters. In <u>AIP</u> Conference Proceedings, volume 321, pages 291–297. American Institute of Physics, 1995.
- [34] Peter L Adair and M Frank Rose. Composite emitters for tpv systems. In <u>AIP Conference Proceedings</u>, volume 321, pages 245–262. American Institute of Physics, 1995.
- [35] Hiroo Yugami, Hitoshi Sai, Kazuya Nakamura, Narihito Nakagawa,

- and Hideki Ohtsubo. Solar thermophotovoltaic using al/sub 2/o/sub 3//er/sub 3/al/sub 5/o/sub 12/eutectic composite selective emitter. In Conference Record of the Twenty-Eighth IEEE Photovoltaic Specialists Conference-2000 (Cat. No. 00CH37036), pages 1214–1217. IEEE, 2000.
- [36] Bernd Bitnar, Wilhelm Durisch, Detlev Grutzmacher, J-C Mayor, Christoph Muller, F Von Roth, JA Anna Selvan, H Sigg, H Rudolf Tschudi, and Jens Gobrecht. A tpv system with silicon photocells and a selective emitter. In <u>Conference Record of the Twenty-Eighth IEEE Photovoltaic Specialists Conference-2000</u> (Cat. No. 00CH37036), pages 1218–1221. IEEE, 2000.
- [37] Lucian G Ferguson and Fatih Dogan. A highly efficient nio-doped mgo matched emitter for thermophotovoltaic energy conversion. Materials Science and Engineering: B, 83(1-3):35–41, 2001.
- [38] B Bitnar, W Durisch, J-C Mayor, H Sigg, and HR Tschudi. Characterisation of rare earth selective emitters for thermophotovoltaic applications. <u>Solar Energy Materials and Solar Cells</u>, 73(3):221–234, 2002.
- [39] Hitoshi Sai, Yoshiaki Kanamori, and Hiroo Yugami. High-temperature resistive surface grating for spectral control of thermal radiation. Applied Physics Letters, 82(11):1685–1687, 2003.
- [40] A Licciulli, D Diso, G Torsello, S Tundo, A Maffezzoli, M Lomascolo, and M Mazzer. The challenge of high-performance selective emitters for thermophotovoltaic applications. <u>Semiconductor</u> science and technology, 18(5):S174, 2003.
- [41] WJ Tobler and W Durisch. Plasma-spray coated rare-earth oxides on molybdenum disilicide—high temperature stable emitters for thermophotovoltaics. <u>Applied energy</u>, 85(5):371–383, 2008.
- [42] WJ Tobler and W Durisch. High-performance selective er-doped yag emitters for thermophotovoltaics. <u>Applied Energy</u>, 85(6):483–493, 2008
- [43] M Araghchini, YX Yeng, N Jovanovic, P Bermel, LA Kolodziejski, M Soljacic, I Celanovic, and JD Joannopoulos. Fabrication of two-dimensional tungsten photonic crystals for high-temperature applications. Journal of Vacuum Science & Technology B, Nanotechnology and Microelectronics: Materials, Processing, Measurement, and Phenomena, 29(6):061402, 2011.
- [44] Veronika Rinnerbauer, Sidy Ndao, Yi Xiang Yeng, Walker R Chan, Jay J Senkevich, John D Joannopoulos, Marin Soljačić, and Ivan Celanovic. Recent developments in high-temperature photonic crystals for energy conversion. <u>Energy & Environmental Science</u>, 5(10): 8815–8823, 2012.
- [45] Yi Xiang Yeng, Michael Ghebrebrhan, Peter Bermel, Walker R Chan, John D Joannopoulos, Marin Soljačić, and Ivan Celanovic. Enabling high-temperature nanophotonics for energy applications. <u>Proceedings of the National Academy of Sciences</u>, 109(7):2280–2285, 2012
- [46] Alejandro Datas and Carlos Algora. Development and experimental evaluation of a complete solar thermophotovoltaic system. <u>Progress in Photovoltaics: Research and Applications</u>, 21(5):1025–1039, 2013.
- [47] Bernd Bitnar, Wilhelm Durisch, and Reto Holzner. Thermophotovoltaics on the move to applications. <u>Applied Energy</u>, 105:430–438, 2013.
- [48] Walker R Chan, Peter Bermel, Robert CN Pilawa-Podgurski, Christopher H Marton, Klavs F Jensen, Jay J Senkevich, John D Joannopoulos, Marin Soljačić, and Ivan Celanovic. Toward highenergy-density, high-efficiency, and moderate-temperature chipscale thermophotovoltaics. Proceedings of the National Academy of Sciences, 110(14):5309–5314, 2013.
- [49] Veronika Rinnerbauer, Yi Xiang Yeng, Walker R Chan, Jay J Senkevich, John D Joannopoulos, Marin Soljačić, and Ivan Celanovic. High-temperature stability and selective thermal emission of polycrystalline tantalum photonic crystals. Optics express, 21(9):11482-11491, 2013.
- [50] Kevin A Arpin, Mark D Losego, Andrew N Cloud, Hailong Ning, Justin Mallek, Nicholas P Sergeant, Linxiao Zhu, Zongfu Yu, Berç Kalanyan, Gregory N Parsons, et al. Three-dimensional self-

- assembled photonic crystals with high temperature stability for thermal emission modification. Nature communications, 4(1):1–8, 2013.
- [51] Andrej Lenert, David M Bierman, Youngsuk Nam, Walker R Chan, Ivan Celanović, Marin Soljačić, and Evelyn N Wang. A nanophotonic solar thermophotovoltaic device. <u>Nature nanotechnology</u>, 9(2): 126–130, 2014.
- [52] Veronika Rinnerbauer, Andrej Lenert, David M Bierman, Yi Xiang Yeng, Walker R Chan, Robert D Geil, Jay J Senkevich, John D Joannopoulos, Evelyn N Wang, Marin Soljačić, et al. Metallic photonic crystal absorber-emitter for efficient spectral control in high-temperature solar thermophotovoltaics. <u>Advanced Energy Materials</u>, 4(12):1400334, 2014.
- [53] Moisés Garín, David Hernandez, Trifon Trifonov, and Ramón Alcubilla. Three-dimensional metallo-dielectric selective thermal emitters with high-temperature stability for thermophotovoltaic applications. Solar Energy Materials and Solar Cells, 134:22–28, 2015.
- [54] Makoto Shimizu, Asaka Kohiyama, and Hiroo Yugami. High-efficiency solar-thermophotovoltaic system equipped with a mono-lithic planar selective absorber/emitter. <u>Journal of Photonics for Energy</u>, 5(1):053099, 2015.
- [55] Craig Ungaro, Stephen K Gray, and Mool C Gupta. Solar thermophotovoltaic system using nanostructures. <u>Optics express</u>, 23 (19):A1149–A1156, 2015.
- [56] Asaka Kohiyama, Makoto Shimizu, and Hiroo Yugami. Unidirectional radiative heat transfer with a spectrally selective planar absorber/emitter for high-efficiency solar thermophotovoltaic systems. Applied Physics Express, 9(11):112302, 2016.
- [57] Walker R Chan, Veronika Stelmakh, Michael Ghebrebrhan, Marin Soljačić, John D Joannopoulos, and Ivan Čelanović. Enabling efficient heat-to-electricity generation at the mesoscale. Energy & Environmental Science, 10(6):1367–1371, 2017.
- [58] Chun-Chieh Chang, Wilton JM Kort-Kamp, John Nogan, Ting S Luk, Abul K Azad, Antoinette J Taylor, Diego AR Dalvit, Milan Sykora, and Hou-Tong Chen. High-temperature refractory metasurfaces for solar thermophotovoltaic energy harvesting. <u>Nano letters</u>, 18(12):7665–7673, 2018.
- [59] Kehang Cui, Paul Lemaire, Hangbo Zhao, Timothy Savas, Gregory Parsons, and A John Hart. Tungsten–carbon nanotube composite photonic crystals as thermally stable spectral-selective absorbers and emitters for thermophotovoltaics. <u>Advanced Energy Materials</u>, 8 (27):1801471, 2018.
- [60] Manohar Chirumamilla, Gnanavel Vaidhyanathan Krishnamurthy, Katrin Knopp, Tobias Krekeler, Matthias Graf, Dirk Jalas, Martin Ritter, Michael Störmer, Alexander Yu Petrov, and Manfred Eich. Metamaterial emitter for thermophotovoltaics stable up to 1400 c. Scientific reports, 9(1):1–11, 2019.
- [61] Jin Hwan Kim, Sang Min Jung, and Moo Whan Shin. Thermal degradation of refractory layered metamaterial for thermophotovoltaic emitter under high vacuum condition. <u>Optics express</u>, 27 (3):3039–3054, 2019.
- [62] Rajendra Bhatt, Ivan Kravchenko, and Mool Gupta. High-efficiency solar thermophotovoltaic system using a nanostructure-based selective emitter. <u>Solar Energy</u>, 197:538–545, 2020.
- [63] Denis G Baranov, Yuzhe Xiao, Igor A Nechepurenko, Alex Krasnok, Andrea Alù, and Mikhail A Kats. Nanophotonic engineering of farfield thermal emitters. <u>Nature materials</u>, 18(9):920–930, 2019.
- [64] David M Bierman, Andrej Lenert, Walker R Chan, Bikram Bhatia, Ivan Celanović, Marin Soljačić, and Evelyn N Wang. Enhanced photovoltaic energy conversion using thermally based spectral shaping. Nature Energy, 1(6):1–7, 2016.
- [65] Veronika Rinnerbauer, Sidy Ndao, Yi Xiang Yeng, Jay J Senkevich, Klavs F Jensen, John D Joannopoulos, Marin Soljačić, Ivan Celanovic, and Robert D Geil. Large-area fabrication of high aspect ratio tantalum photonic crystals for high-temperature selective emitters. Journal of Vacuum Science & Technology B, Nanotechnology and Microelectronics: Materials, Processing, Measurement, and Phenomena, 31(1):011802, 2013.
- [66] Masahiro Suemitsu, Takashi Asano, Takuya Inoue, and Susumu

- Noda. High-efficiency thermophotovoltaic system that employs an emitter based on a silicon rod-type photonic crystal. <u>ACS Photonics</u>, 7(1):80–87, 2019.
- [67] ES Sakr, Zhiguang Zhou, and Peter Bermel. High efficiency rareearth emitter for thermophotovoltaic applications. <u>Applied Physics</u> <u>Letters</u>, 105(11):111107, 2014.
- [68] Nghia Nguyen-Huu, Yu-Bin Chen, and Yu-Lung Lo. Development of a polarization-insensitive thermophotovoltaic emitter with a binary grating. Optics express, 20(6):5882–5890, 2012.
- [69] Jinlin Song, Hao Wu, Qiang Cheng, and Junming Zhao. 1d trilayer films grating with w/sio2/w structure as a wavelength-selective emitter for thermophotovoltaic applications. <u>Journal of Quantitative</u> Spectroscopy and Radiative Transfer, 158:136–144, 2015.
- [70] Y-B Chen and ZM Zhang. Design of tungsten complex gratings for thermophotovoltaic radiators. <u>Optics communications</u>, 269(2):411– 417, 2007.
- [71] Chihhui Wu, Burton Neuner III, Jeremy John, Andrew Milder, Byron Zollars, Steve Savoy, and Gennady Shvets. Metamaterial-based integrated plasmonic absorber/emitter for solar thermo-photovoltaic systems. Journal of Optics, 14(2):024005, 2012.
- [72] Bo Zhao, Liping Wang, Yong Shuai, and Zhuomin M Zhang. Ther-mophotovoltaic emitters based on a two-dimensional grating/thin-film nanostructure. <u>International Journal of Heat and Mass Transfer</u>, 67:637–645, 2013.
- [73] Hong Ye, Hujun Wang, and Qilin Cai. Two-dimensional vo2 photonic crystal selective emitter. <u>Journal of Quantitative Spectroscopy</u> and Radiative Transfer, 158:119–126, 2015.
- [74] Zhiguang Zhou, Omar Yehia, and Peter Bermel. Integrated photonic crystal selective emitter for thermophotovoltaics. <u>Journal of Nanophotonics</u>, 10(1):016014, 2016.
- [75] Enas Sakr and Peter Bermel. Thermophotovoltaics with spectral and angular selective doped-oxide thermal emitters. <u>Optics express</u>, 25 (20):A880–A895, 2017.
- [76] Tun Cao, Lei Zhang, Robert E Simpson, and Martin J Cryan. Midinfrared tunable polarization-independent perfect absorber using a phase-change metamaterial. JOSA B, 30(6):1580–1585, 2013.
- [77] Sean Molesky, Christopher J Dewalt, and Zubin Jacob. High temperature epsilon-near-zero and epsilon-near-pole metamaterial emitters for thermophotovoltaics. Optics express, 21(101):A96–A110, 2013.
- [78] Huixu Deng, Tianchen Wang, Jie Gao, and Xiaodong Yang. Metamaterial thermal emitters based on nanowire cavities for highefficiency thermophotovoltaics. <u>Journal of Optics</u>, 16(3):035102, 2014.
- [79] Jui-Yung Chang, Yue Yang, and Liping Wang. Tungsten nanowire based hyperbolic metamaterial emitters for near-field thermophotovoltaic applications. <u>International Journal of Heat and Mass</u> Transfer, 87:237–247, 2015.
- [80] Vidya Ganapati, T Patrick Xiao, and Eli Yablonovitch. Ultraefficient thermophotovoltaics exploiting spectral filtering by the photovoltaic band-edge. arXiv preprint arXiv:1611.03544, 2016.
- [81] Richard M Swanson. Silicon photovoltaic cells in thermophotovoltaic energy conversion. In 1978 International Electron Devices Meeting, pages 70–73. IEEE, 1978.
- [82] Tobias Burger, Dejiu Fan, Kyusang Lee, Stephen R Forrest, and Andrej Lenert. Thin-film architectures with high spectral selectivity for thermophotovoltaic cells. ACS Photonics, 5(7):2748–2754, 2018.
- [83] Patrick M Fourspring, David M DePoy, Thomas D Rahmlow Jr, Jeanne E Lazo-Wasem, and Edward J Gratrix. Optical coatings for thermophotovoltaic spectral control. <u>Applied optics</u>, 45(7):1356– 1358, 2006.
- [84] Bernard Wernsman, Richard R Siergiej, Samuel D Link, Robert G Mahorter, Marc N Palmisiano, Rebecca J Wehrer, Robert W Schultz, Gregory P Schmuck, Rowan L Messham, Susan Murray, et al. Greater than 20% radiant heat conversion efficiency of a thermophotovoltaic radiator/module system using reflective spectral control. IEEE Transactions on Electron Devices, 51(3):512–515, 2004.
- [85] H Ehsani, I Bhat, J Borrego, R Gutmann, E Brown, R Dzeindziel, M Freeman, and N Choudhury. Characteristics of degenerately

- doped silicon for spectral control in thermophotovoltaic systems. In AIP Conference Proceedings, volume 358, pages 312–328. American Institute of Physics, 1996.
- [86] David DePoy, Patrick Fourspring, Edward Brown, Thomas Rahmlow, Jeanne Lazo-Wassem, and Edward Gratrix. Thermophotovoltaic spectral control. In <u>2nd International Energy Conversion</u> Engineering Conference, page 5762, 2004.
- [87] Yi Xiang Yeng, Walker R Chan, Veronika Rinnerbauer, John D Joannopoulos, Marin Soljačić, and Ivan Celanovic. Performance analysis of experimentally viable photonic crystal enhanced thermophotovoltaic systems. Optics express, 21(106):A1035-A1051, 2013
- [88] Christopher J Crowley, Nabil A Elkouh, Susan Murray, and Donald L Chubb. Thermophotovoltaic converter performance for radioisotope power systems. In AIP Conference Proceedings, volume 746, pages 601–614. American Institute of Physics, 2005.
- [89] Alina LaPotin, Kevin L Schulte, Myles A Steiner, Kyle Buznitsky, Colin C Kelsall, Daniel J Friedman, Eric J Tervo, Ryan M France, Michelle R Young, Andrew Rohskopf, et al. Thermophotovoltaic efficiency of 40%. arXiv preprint arXiv:2108.09613, 2021.
- [90] John R Howell, M Pinar Mengüç, Kyle Daun, and Robert Siegel. Thermal radiation heat transfer. CRC press, 2020.
- [91] Lucian G Ferguson and Fatih Dogan. Spectral analysis of transition metal-doped mgo "matched emitters" for thermophotovoltaic energy conversion. Journal of materials science, 37(7):1301–1308, 2002.
- [92] S Bitnar, W Durisch, G Palfinger, F Von Roth, U Vogt, A Brönstrup, and D Seiler. Practical thermophotovoltaic generators. Semiconductors, 38(8):941–945, 2004.
- [93] Nicole A Pfiester and Thomas E Vandervelde. Selective emitters for thermophotovoltaic applications. <u>Physica status solidi (a)</u>, 214(1): 1600410, 2017.
- [94] Pavel N Dyachenko, Sean Molesky, A Yu Petrov, Michael Störmer, Tobias Krekeler, Slawa Lang, Martin Ritter, Zubin Jacob, and Manfred Eich. Controlling thermal emission with refractory epsilon-near-zero metamaterials via topological transitions. <u>Nature</u> communications, 7(1):1–8, 2016.
- [95] Werner Martienssen and Hans Warlimont. Springer handbook of condensed matter and materials data. Springer Science & Business Media, 2006.
- [96] Ihsan Barin and Gregor Platzki. Thermochemical data of pure substances, volume 304. Wiley Online Library, 1989.
- [97] Heon-Ju Lee, Katherine Smyth, Stephen Bathurst, Jeffrey Chou, Michael Ghebrebrhan, John Joannopoulos, Nannaji Saka, and Sang-Gook Kim. Hafnia-plugged microcavities for thermal stability of selective emitters. <u>Applied Physics Letters</u>, 102(24):241904, 2013.
- [98] Daniel Peykov, Yi Xiang Yeng, Ivan Celanovic, John D Joannopoulos, and Christopher A Schuh. Effects of surface diffusion on high temperature selective emitters. <u>Optics express</u>, 23(8):9979–9993, 2015.
- [99] Kevin A Arpin, Mark D Losego, and Paul V Braun. Electrodeposited 3d tungsten photonic crystals with enhanced thermal stability. Chemistry of Materials, 23(21):4783–4788, 2011.
- [100] Manohar Chirumamilla, Gnanavel Vaidhyanathan Krishnamurthy, Surya Snata Rout, Martin Ritter, Michael Störmer, Alexander Yu Petrov, and Manfred Eich. Thermal stability of tungsten based metamaterial emitter under medium vacuum and inert gas conditions. <u>Scientific reports</u>, 10(1):1–10, 2020.
- [101] Gnanavel Vaidhyanathan Krishnamurthy, Manohar Chirumamilla, Surya Snata Rout, Kaline P Furlan, Tobias Krekeler, Martin Ritter, Hans-Werner Becker, Alexander Yu Petrov, Manfred Eich, and Michael Störmer. Structural degradation of tungsten sandwiched in hafnia layers determined by in-situ xrd up to 1520° c. <u>Scientific</u> reports. 11(1):1–12, 2021.
- [102] Jeffrey B Chou, Yi Xiang Yeng, Yoonkyung E Lee, Andrej Lenert, Veronika Rinnerbauer, Ivan Celanovic, Marin Soljačić, Nicholas X Fang, Evelyn N Wang, and Sang-Gook Kim. Enabling ideal selective solar absorption with 2d metallic dielectric photonic crystals. Advanced Materials, 26(47):8041–8045, 2014.

- [103] Zhiguang Zhou, Hao Tian, Thomas M Hymel, Harsha Reddy, Vladimir M Shalaev, Yi Cui, and Peter Bermel. High-temperature, spectrally-selective, scalable, and flexible thin-film si absorber and emitter. Optical Materials Express, 10(1):208–221, 2020.
- [104] Jin Hwan Kim, Sang Min Jung, and Moo Whan Shin. High-temperature degradation of one-dimensional metallodielectric (w/sio2) photonic crystal as selective thermal emitter for thermophotovoltaic system. Optical Materials, 72:45–51, 2017.
- [105] Matthew P Wells, Ryan Bower, Rebecca Kilmurray, Bin Zou, Andrei P Mihai, Gomathi Gobalakrichenane, Neil McN Alford, Rupert FM Oulton, Lesley F Cohen, Stefan A Maier, et al. Temperature stability of thin film refractory plasmonic materials. <u>Optics express</u>, 26(12):15726–15744, 2018.
- [106] William W Mullins. Theory of thermal grooving. <u>Journal of Applied</u> Physics, 28(3):333–339, 1957.
- [107] Nicholas R Denny, Sang Eon Han, David J Norris, and Andreas Stein. Effects of thermal processes on the structure of monolithic tungsten and tungsten alloy photonic crystals. <u>Chemistry of</u> Materials, 19(18):4563–4569, 2007.
- [108] C Schlemmer, J Aschaber, V Boerner, and J Luther. Thermal stability of micro-structured selective tungsten emitters. In <u>AIP Conference Proceedings</u>, volume 653, pages 164–173. American Institute of Physics, 2003.
- [109] Veronika Stelmakh, Daniel Peykov, Walker R Chan, Jay J Senkevich, John D Joannopoulos, Marin Soljačić, Ivan Celanovic, Robert Castillo, Kent Coulter, and Ronghua Wei. Thick sputtered tantalum coatings for high-temperature energy conversion applications.

 Journal of Vacuum Science & Technology A: Vacuum, Surfaces, and Films, 33(6):061204, 2015.
- [110] Bancha Kongtragool and Somchai Wongwises. A review of solar-powered stirling engines and low temperature differential stirling engines. Renewable and Sustainable energy reviews, 7(2):131–154, 2003
- [111] Thomas Mancini, Peter Heller, Barry Butler, Bruce Osborn, Wolfgang Schiel, Vernon Goldberg, Reiner Buck, Richard Diver, Charles Andraka, and James Moreno. Dish-stirling systems: An overview of development and status. J. Sol. Energy Eng., 125(2):135–151, 2003.
- [112] Uday Raj Singh and Anil Kumar. Review on solar stirling engine: Development and performance. <u>Thermal Science and Engineering</u> Progress, 8:244–256, 2018.